Travail de fin d'études et stage[BR]- Travail de fin d'études : Characterization and Modelling of a two-phase expander in an Organic Rankine Cycle[BR]- Stage d'insertion professionnelle : National Technical University of Athens

Auteur : Neven, Elise
Promoteur(s) : Lemort, Vincent
Faculté : Faculté des Sciences appliquées
Diplôme : Master en ingénieur civil électromécanicien, à finalité spécialisée en énergétique
Année académique : 2022-2023
URI/URL : http://hdl.handle.net/2268.2/18130

University of Liege
Faculty of Applied Sciences
Academic year 2022-2023

National Technical
University of Athens

Characterization and Modelling of a two-phase expander in an Organic Rankine Cycle

Master thesis submitted in partial fulfillment of the requirements for the Master's degree in Electromechanical Engineering

by **Neven Elise**

Promotor:
LEMORT Vincent

Jury:
LEMORT Vincent
KARELLAS Sotirios
GENDEBIEN Samuel

Supervisors:
LECLERCQ Nicolas
LEONTARITIS Aris

Abstract

Energy production and consumption play an essential role in climate change and reducing the greenhouse gas emissions coming from that sector is essential. The European Union has set out ambitious targets for 2030 and 2050 to mitigate climate change and in the perspective of reaching these goals, the EU has developed the ”Horizon Europe” program. ”Horizon Europe” is a funding program to finance research and innovation and one of its fields is Energy. REGEN-BY-2 (Next REnewable multi-GENeration technology enabled by TWO-phase fluids machines) is one of the initiatives launched by ”Horizon Europe”. This energy plant is capable of converting any type of thermal Renewable Energy Sources into energy vectors such as electric, heating and-or cooling powers. This thesis focuses on one of the main difficulties that take place in this energy plant which is the two-phase expansion.

The first objective of this thesis is the characterization of a commercial scroll expander performance in the two-phase region. A test bench of an Organic Rankine Cycle with a two-phase expansion is built to conduct the experimental campaigns. The main operational variables that impact the expander are varied i.e. the vapor quality, the pressure ratio, the inlet pressure and the expander speed. To analyze the experimental results, a tool allowing to perform a Gaussian regression is used. The main conclusions withdrawn from the experimental results are that the isentropic and volumetric efficiencies decrease with decreasing vapor quality. Another observation is that the under-expansion losses appear to be emphasized when working with lower vapor quality.
The second objective is the prediction of the performance outside of the test range. For this purpose, a semi-empirical model of the expander working in two-phase is proposed, calibrated with the experimental data. This model allows to analyze the performance of the expander outside of the test range.

Acknowledgments

I would like to first thank my supervisor, Professor V. Lemort, for giving me the opportunity to realize my thesis in Athens and for his guidance.

I would also like to thank all the members of the thermodynamics and transport phenomena laboratory of the National Technical University of Athens for their welcome. A particular thanks to Aris Leontaritis for sharing his knowledge on the test bench and for his explanations on the post-processing, to Tryfonas Roumpedakis for carrying out experimental campaigns and showing me the working principle of the test bench and to Stratis for his advice in the post-processing codes. I am extremely thankful to Professor Sotirios Karellas for welcoming me in the laboratory.

I would like to particularly thank Nicolas Leclercq from the Thermodynamics Laboratory of Liege for the countless times dedicated to this thesis, the valuable advice and the many rereadings.

Finally, I would like to deeply thank my family, my partner and my friends (from Belgium and from Greece) for their unfailing support.

Contents

List of Figures

List of Tables

Nomenclature

Acronyms

EU European Union

REGEN-BY-2 Next REnewable multi-GENeration technology enabled by TWO phase fluids machines

RES Renewable Energy Sources

ORC Organic Rankine Cycle

TFC Trilateral Flash Cycle

NTUA National Technical University of Athens

OCR Oil Circulation Ratio

VFD Variable Frequency Drive

HVAC Heating, Ventilation and Air Conditioning

HEX Heat Exchanger

COP Coefficient of Performance

RTD Resistive Temperature Detectors

GUI Graphic User Interface

GP Gaussian Processes

MAE Mean Absolute Error

CV Cross Validation

Symbols

Δ Difference

$r_{v,in}$ Built-in volume ratio [-]

V_s Swept volume [cm^3]

$SVFR$ Specific Volumetric Fluid Ratio [-]

$\dot{m}$ Mass flow rate [kg/s]

ρ Density [kg/m^3]

M Mach number [-]

C_p Specific heat enthalpy [kJ/kgK]

h Specific enthalpy [kJ/kg]

s Specific entropy [kJ/Tkg]

v Specific volume [m^3/kg]

P Pressure [bar]

T Temperature [K]

N Speed [RPM]

r_p Pressure ratio [-]

Q Vapor quality [-]

$\dot{Q}$ Thermal capacity [W]

$\dot{W}$ Mechanical power [W]

ε_{is} Isentropic efficiency [-]

ε_v Volumetric efficiency [-]

d Diameter [mm]

AU Heat transfer coefficient [W/K]

A Area [mm^3]

T Torque [N-m]

Subscripts

w Water

r Refrigerant

in Inlet

out Outlet

ev Evaporator

exp Expander

sh Shaft

gen generator

liq Liquid sate

vap Vapor sate

σ Saturated state

is Isentropic

th Theroritical

su Supply

ex Exhaust

leak Leakages

thr Throat

calc Calculated

pred Predicted

meas Measured

Chapter 1

Introduction

Energy production and consumption play an essential role in climate change. Indeed, the energy sector represents more than 75% of the European Union (EU)'s greenhouse gas emissions. With the increase in energy demand, reducing greenhouse gas emissions from energy production and consumption is essential in mitigating climate change. This can be done through the use of renewable energy, the improvement of energy efficiency, the use of storage, and reducing our overall energy consumption.

The EU has set out ambitious targets for 2030 and 2050 to mitigate the climate change issue; decreasing at least 55% greenhouse gas emissions compared to 1990 by 2030 and becoming a neutral climate continent by 2050. In 2018, the European Commission established the binding target to increase to at least 32% the part of renewable energy production in the overall energy mix by 2030.[1]

In the perspective of reaching these goals, the EU has developed a series of programs among which is the "Horizon Europe". Horizon Europe is a funding program put in place until 2027 to finance research and innovation. The funding priorities of Horizon Europe encompass a broad spectrum of fields, including "Climate, Energy, and Mobility". [2]

1.1 REGEN-BY-2

1.1.1 Project description

In September 2020, the Horizon Europe initiative launched one new project called **REGEN-BY-2** which stands for Next REnewable multi-GENeration technology enabled by TWO-phase fluids machines. The proposed energy plant is capable of converting any type of thermal Renewable Energy Source (RES), from low to high-temperature like solar, aerothermal, geothermal, hydrothermal, and additional thermal sources such as waste heat into energy vectors

such as electric, heating and-or cooling powers. This enables the simultaneous supply of different types of end-users with varying energy demands and the plant possesses thus a large flexibility. Thanks to its high flexibility, the energy plant will be able to meet the end-users' demands with high precision, as to decrease energy losses. The thermodynamic cycle is highly efficient as it is based on a combination of nearly direct and inverse Carnot cycles, enabled by two-phase fluids machines. Compared to the well-known Rankine cycle, REGEN-BY-TWO can take advantage of lower heating temperature sources and increase the power output by 50 %.[3]

1.1.2 Thermodynamic cycle

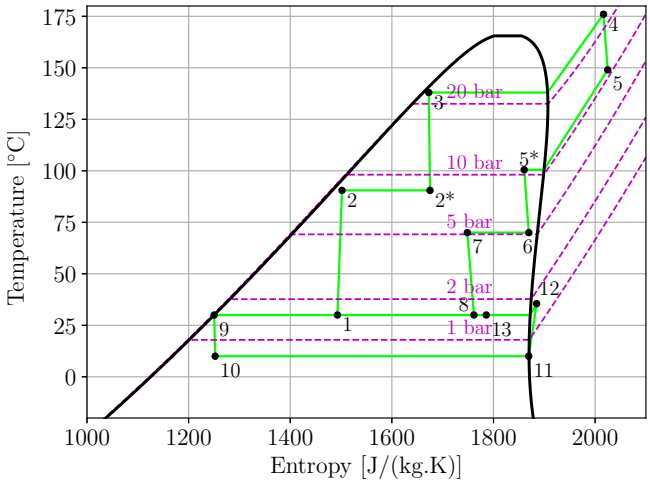

Figure 1.1: *Temperature - specific entropy diagram of the Regen-by-two power plant.*

In **Figure 1.1**, the temperature-entropy thermodynamic cycle of the energy plant of the REGEN-BY-2 project is represented.
In this cycle, a working fluid (HFO R1233zd) circulates and supplies the end-users with electric power, heating power and cooling power. The overall flow rate is divided into two shares, which circulate in two subcircuits; C1 (lines 1-2-2'-3-4-5-5'-6-7-8) and C2 (lines 1-9-10-11-13).

- 1 $\rightarrow$ 2, 2' $\rightarrow$ 3 and 11 $\rightarrow$ 12: Work is provided to the working fluid via two-phase compression machines.
- 3 $\rightarrow$ 4: The heat sources provided by the RES heat the working fluid through a vapor generator.
- 6 $\rightarrow$ 7: Heating power is provided to the end-users.
- 4 $\rightarrow$ 5: Electric power is provided to the end-users via one-phase expansion machines.

- 5' $\rightarrow$ 6 and 7 $\rightarrow$ 8: Electric power is provided to the end-users via two-phase expansion machines.
- 10 $\rightarrow$ 11: Cooling power is provided to the end-users.

Many challenges are present in the realization of the REGEN-BY-2 project. One of the main characteristics of the cycle is the expansions and compressions that take place in the two-phase region (i.e. the working fluid is composed of vapor and liquid phases). To be successful, those two-phase machines have to be designed, prototyped and integrated. This thesis focuses on the two-phase expanders necessary to realize this cycle. Two two-phase expansions are present in the cycle and the thermodynamic points between which the expansions take place are represented in **Table 1.1**.

Table 1.1: *Points on which the two-phase expansions take place.*

Points	Pressure [bar]	Vapour quality [-]
5'	11.2	0.897
6	5.4	0.965
7	5.4	0.713
8	1.6	0.822

The '7$\rightarrow$ 8' expansion is the only one tested with the test bench described in Chapter 3.

1.2 Aim of the thesis

The aim of the thesis is the characterization of the commercial expander in the two-phase region integrated into an Organic Rankine Cycle (ORC). The ORC with the two-phase expansion is fully equipped with sensors to characterize its behavior and experimental tests are carried out to test its performance. The purpose of testing this commercial scroll expander is to test its behavior in the two-phase regions to help the construction of a scroll expander designed specifically for two-phase flows. The second objective is to predict the performance of the expander outside of the testing range via a semi-empirical model.

1.3 Overview

This thesis is organized into several chapters:

- **Chapter 1:** The introduction provides the context and the project for which this thesis has been realized.
- **Chapter 2:** A state of the art on two-phase expander is provided, to give an idea of the theoretical knowledge and experimental advancement of this technology.

- **Chapter 3:** A description of the experimental setup is provided. The ORC unit, the secondary loops, the sensors and the data acquisition system are described.
- **Chapter 4:** A complete analysis of the experimental results is conducted as well as the use of a Gaussian prediction tool.
- **Chapter 5:** The performances of the scroll expander in the two-phase region are predicted through an experimental model.
- **Chapter 6:** Conclusions are drawn and some perspectives to improve the work are proposed.

Chapter 2

State of the art on two-phase expanders

This section proposes an overview of the rare scientific literature available on two-phase expanders. This state-of-the-art is based on a review already made on two-phase expanders by Francesconi et al. (2021) [4].

2.1 Two-phase expanders

2.1.1 Introduction

An expander is a device that converts the energy stored in a high-pressure gas into useful work. The performance of the expander determines the efficiency of the whole thermodynamic cycle and is especially important. Its efficacity is measured with respect to the isentropic expansion i.e. without losses.
Two main families of expanders exist; dynamical and volumetric. Dynamical expanders (also called turbines) convert the pressure energy into kinetic energy to drive the impeller connected to a shaft. Volumetric expanders utilize the pressure energy of the trapped fluid to expand the volume of the fluid in the working chamber to move the shaft. Small scales applications are not suitable for turbomachines as the rotational speeds are very high and their costs increase at these sizes. For these applications, volumetric machines are preferred as they turn at lower rotational speeds and are less expensive for small scales applications.
The research on two-phase expanders focuses mainly on volumetric expanders. Indeed, volumetric expanders possess a greater tolerance to low fluid quality and for application in two-phase flows, having a lower rotational speed is necessary.
Volumetric expanders are composed of one static part and one or several moving parts that drive a mechanical shaft. The inner surfaces of these parts shape one or several working chambers whose volume variation is due to the relative motion between the static and moving surface. Two types of volumetric expanders exist depending on the motion shaft; alternative (piston) and rotating (screws, scrolls, and rotating vanes). As Dumont et al. (2018) [5] states, piston expanders are not well suited for two-phase applications as they are less toler-

ant to droplets and they possess high friction loss. The focus is thus on rotating volumetric expanders such as the scroll expander, screw and root expander. The available literature on two-phase expanders is mainly on scroll and twin-screw expanders, thus, this state-on-the-art only reviews those two technologies. During two-phase expansion, a variation of the mass of both liquid and vapor phases take place, i.e. the quality of the working fluid changes. This requires non-conventional technologies. At the moment, the two-phase expander remains largely in the theoretical domain. As explained in section 2.3, two-phase expansion has multiple possible applications, however, for it to be interesting, the expansion has to be efficient.

2.1.2 Volumetric expanders working principle

The actual operation of an expander differs from the isentropic one mainly due to under- and over-expansion. Two parameters characterize the expansion process; the Built-in volume ratio $r_{v,in}$ ($r_{v,in} = \frac{V_{out}}{V_{in}}$ where V_{out} and V_{in} are the outlet and inlet volume respectively) which depends only on the expander geometry; and the Specific Volumetric Fluid Ratio SVFR ($SVFR = \frac{v_{out}}{v_{in}}$ where v_{out} and v_{in} are the outlet and inlet specific volume respectively) that is determined by the operating conditions. When the $r_{v,in}$ and the SVFR match, there are no under- or over-expansion. When the $r_{v,in}$<SVFR, there is an under-expansion and the discharge pressure (determined by the $r_{v,in}$) is higher than the exhaust pressure (determined by the operating conditions). When the $r_{v,in}$>SVFR, there is an over-expansion and the discharge pressure is lower than the exhaust pressure (see **Figure 2.1**).

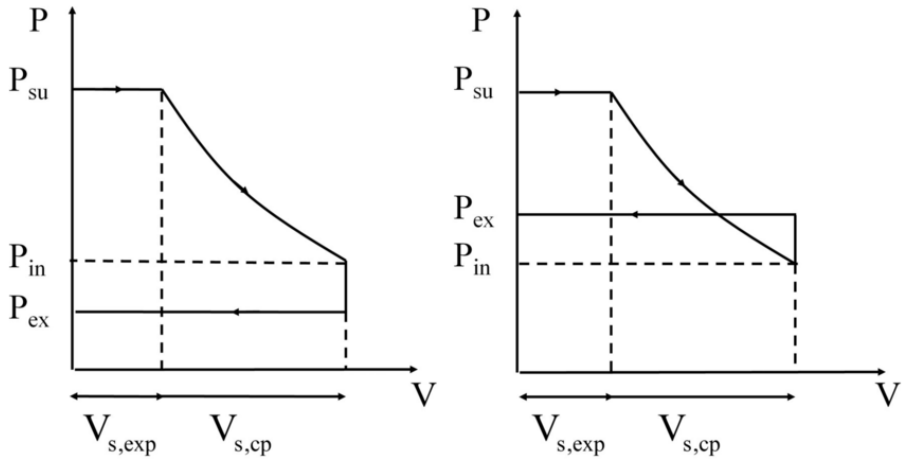

Figure 2.1: *Over and under expansion Pressure-Volume diagram. (source :[6])*

Additionally, other losses are also to take into consideration; internal fluid leakages, pressure losses in the ports, heat transfer losses, and friction losses.

2.1.3 Drawbacks and advantages of two-phase expanders

The use of two-phase expanders instead of single-phase expanders presents some advantages as well as some disadvantages.

Advantages

- Depending on the working fluid, a single-phase volumetric expander usually requires lubrication and a dedicated circuit for the oil circulation (including a separator and a pump). Nonetheless, the oil can potentially mix with the working fluid which could reduce the lubrication capacity and thus increase the friction losses and the wear on the machine. On the other side, two-phase volumetric expanders could potentially eliminate the necessity for lubricating oil, as the liquid phase of the working fluid could serve as a lubricant for surfaces.
- The liquid phase may act as a sealant by blocking the gap between the working chambers which would reduce the leakages and increase the volumetric efficiency.
- In [7], Briola et al. (2012) found that two-phase expanders produce higher mechanical power compared to homologous single-phase machines with the same mass flow rate, inlet pressure, outlet pressure, and fluid quality at the inlet.
- Two-phase expansion gets closer to an isothermal process, decreasing the thermal stress on the moving parts and maximizing the work produced by the expander.

Disadvantages

- The mechanical reliability of the machine is questioned due to the presence of liquid. The lifetime of the two-phase expander could be limited due to the decrease in the viscosity of the refrigerant-oil mixture.
- Two sources of losses could have more impact when working with two-phase flows. First, an increase in the pressure losses in the suction/discharge ports due to the decrease of the speed of sound or the increase in density. There is also a loss of mechanical efficiency resulting from the higher viscosity of the liquid phase in contact with the moving parts.
- To determine the performances of a two-phase volumetric expander, thermal equilibrium between the liquid and the vapour phase during the expansion process is required. However, the expansion process takes a short time, and a thermal equilibrium only exists if there is a large enough heat exchange surface between the two-phase. The working fluid needs to be constituted by fine liquid particles uniformly dispersed in the two-phase region. [7]
- The heat exchange coefficient of a two-phase flow is higher than that of a vapor-phase flow. This results in higher thermal losses between the flow and the machine surfaces. The expander needs better insulation.

Flashing in two-phase flows

Another phenomenon that could impair the performance of two-phase expanders is the flashing phenomenon. Flash evaporation is a phenomenon that takes place in liquid or two-phase flows that undergoes a pressure decrease. It is defined by a phase change that occurs in the flow when the pressure goes below the saturation pressure, thus increasing the vapor quality. In two-phase expansion, flashing happens during the suction and the expansion process due to a pressure decrease. The flashing phenomena happening in two-phase expanders see the volume of the flashing chamber varying over time. This kind of flashing is almost not mentioned in the literature. Kanno et al. (2015) and Lecompte et al. (2107), have established that flashing evaporation is a non-equilibrium process because it entails the formation of bubbles that increase in number and size over the expansion [8] [9]. The thermal disequilibrium between the vapor and liquid phases during the expansion penalizes the efficiency of the expander. The pressure change results in high-density variation in the vapor phase and thus a high-temperature variation, while the density and temperature change is negligible in the liquid phase. However, high efficiency in a two-phase expander can only be obtained if the temperature of the two phases is matching (i.e. thermal equilibrium) and this requires an adequate heat exchange between them.

2.2 Volumetric expanders working with two-phase flows

2.2.1 Two-phase scroll expander

Working principle

The scroll expander is composed of one fixed scroll and one orbiting scroll (**Figure 2.2**). At the center of the expander is the suction chamber which communicates with the supply. Fluid is admitted into that suction chamber and forms a pocket of fluid. The volume of the pocket of fluid is increased from the minimum clearance volume until the exhaust volume over one expander shaft revolution. The volume increase decreases the pressure from the supply pressure until the internal pressure (defined by the volume ratio given by the manufacturer). The mechanical power is available at the crankshaft linked with the orbiting spiral. Scroll expanders have multiple advantages. First, the machine is capable of expanding efficiently at high-pressure ratios, even at low rotational speeds. Due to the reduced number of moving parts, it is reliable and robust as it is very simple. The isentropic efficiency is also very high.

The scroll expander is usually not commercially available. Fortunately, a scroll compressor can be changed into an expander by making it run in reverse and by removing the reed valves that prevent the creation of backflow in the compressor (Dumont et al., 2014 [10]).

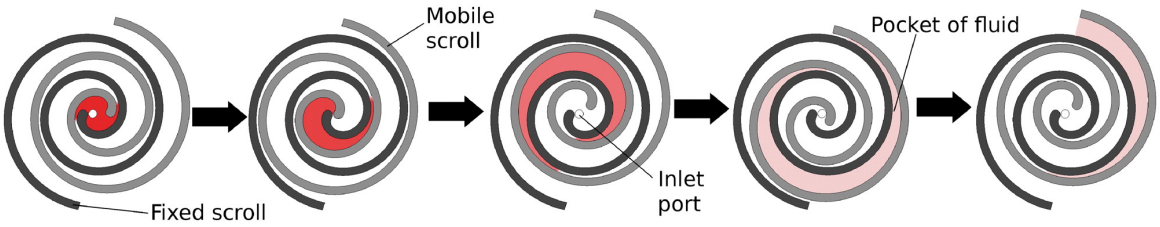

Figure 2.2: *Working principle of a scroll expander. (source :[11]*

Applications of the scroll expander with two-phase flows

This section provides a list of the main experimental and theoretical studies already made on two-phase scroll expanders.

The first applications of the two-phase scroll expanders began in the early 2000s but were mainly numerical simulations on two-phase expanders in vapor compression refrigeration cycles with CO_2 as the working fluid. The first study was conducted by Huff et al. (2002) [12]. They developed an algorithm to estimate the performance of compression and expansion processes within positive displacement machines. The algorithm's applications extend beyond component performance estimation, enabling in-depth investigations into enhancing the overall efficiency of vapor compression cycles through integrated compressor-expander devices. In the same periods, Westphalen et al. (2006) [13] developed a scroll expander design for integration with a dual-stage rotary compressor for use in CO_2 cooling cycles. They built a proof-of-concept prototype based on the design concept developed by CFD (Computational Fluid Dynamics) and FEM (Finite Element Method) analysis, with a displacement volume of 2.3 cm^3 and a volume expansion ratio of 2. Leakage testing under static conditions was conducted to investigate the primary potential causes of energy loss in the expander, particularly focusing on CO_2 leakage through the expander. The results of this testing indicate that the leakage is controllable and remains within acceptable limits, not exceeding 10% of the designed expander flow. That prototype was later tested by H. Kohsokabe et al. (2008) [14] to investigate the basic operating characteristics of the CO_2 refrigeration cycle. The inclusion of the expander-compressor unit led to an enhanced coefficient of performance (COP) for the CO_2 chiller cycle in both cooling and heating scenarios. The COP improvement achieved with the expander-compressor unit exceeded 30%, with an overall efficiency of the unit reaching 57%.
In 2006, Fukuta et al. [15] conducted both theoretical and practical examinations on a prototype of a two-phase scroll expander in a CO_2 refrigeration cycle. Calculation results indicated that, with a 10 μm leakage clearance and a rotational speed of 3600 rpm, the scroll expander achieved approximately 0.6 total efficiency. The prototyped scroll expander was constructed using a scroll compressor component from a water heater, yielding an 0.8 volumetric efficiency and an overall total efficiency of around 0.55, even without significant modifications

to the compressor's scroll element.
In 2008, Hiwata et al. [16] created a prototype of a two-phase scroll expander for CO_2 refrigerant and integrated strategies to minimize radial and flank leakages. Specifically, the reduction in radial leakages was achieved by implementing over-expansion. This approach prevented the separation of the orbiting spiral from the stationary one, even when the operating conditions changed. The decrease in flank leakages was accomplished through a mechanism that utilized oil-film pressure on the shaft bearing to compel the orbiting spiral to remain in contact with the fixed spiral.
In 2008, Kim et al. [17] investigated the integration of a combined scroll expander-compressor unit in a two-stage compression CO_2 trans-critical cycle to enhance the cycle's COP. The two-phase scroll expander was employed to directly power the initial stage compressor of a two-stage intercooled compressor system. The results were compelling as the main compressor's energy input could be decreased by 12.1$\%$ due to the expander power output. Consequently, the cycle's COP was projected to improve by 23.5$\%$ with the implementation of this expander-compressor unit. The last investigation related to the implementation of two-phase scroll expanders within CO_2 vapor compression refrigeration cycles was conducted in 2010 by Kakuda et al. [18]. Specifically, they designed a prototype of a two-phase scroll expander to directly power the second-stage compressor of a two-stage intercooled compressor setup. The experimental results yielded a volumetric efficiency range of 0.97 to 1.54. The excess above 100$\%$ was attributed to pressure losses at the inlet port, as well as close-range, interactions between the fixed and orbiting wraps of the expander.

Another application of two-phase scroll expanders was explored in the late 2000s, in the context of the wet vapor Rankine cycle, using water as the working fluid.
In 2007, Kim et al. [19] developed a prototype of the two-phase scroll expander intended for generating power from a steam source with relatively low temperatures. The expander employs a dual-sided orbiting scroll mechanism, eliminating the need for a thrust bearing to support the base plate of the moving scroll. Through experimentation involving the scroll expander prototype with a scroll clearance of approximately 64 μm, data was collected on mass flow rate and shaft power output. This analysis revealed a volumetric efficiency ranging from 0.42 to 0.52., and a consistent total expander efficiency at around 0.34 across shaft speeds ranging from 1000 to 1400 RPM. In 2011, ECR International developed two variations of two-phase scroll expanders designed for applications in a wet vapor Rankine cycle. This cycle employed water as the working fluid and was utilized for cogeneration purposes. [20]

2.2.2 Two-Phase Twin Screw Expander

Working principle

The twin screw expander is composed of two embedded screws (one male and one female) fixed on parallel axes that rotate in opposite senses. The male rotor is made up of lobes while the female rotor is made up of flutes. They are both attached at the end by bearings. To avoid direct contact, timing gears can be used to synchronize the rotation of the screws. To minimize internal leakages, the screw profiles must form a good seal between each other and between the casing at all rotational positions.

At the beginning of the expansion, the screws and the casing form an expansion chamber that is in communication with the inlet port. During the following expansion, the inlet and outlet port stay closed while the expansion chamber volume increases progressively, moving along the screws. The fluid static pressure applies a force on the rotors causing their rotations which creates the mechanical work, available on the shaft. Finally, the expansion chamber is discharged through the outlet port.

Figure 2.3: *Working principle of a twin screw expander. (source :[21]*

Applications of the twin screw expander with two-phase flows

Two-phase screw expanders were mainly developed for application in power cycles (such as the direct expansion of a geothermal fluid, TFC, and a wet vapor Rankine cycle).

The first study related to two-phase screw expanders was conducted in the 1970s thanks to Sprankle [22]. He conceived a two-phase twin screw expander for the direct expansion of a geothermal fluid.
In 1996, Smith et al. provided a numerical analysis of Sprankle's two-phase expanders working with water to explain their poor performances and improve their operation [23]. They carried out an experimental campaign to validate this model by testing several machines working with R113. They pointed out the greater pressure drops in the intake ports due to the increased fluid density when working with two-phase fluid. The same authors theo-

retically investigated in 2005 the application of a two-phase twin screw expander for direct expansion of a geothermal fluid [24]. They found out the Built-in volume ratio depends exclusively on the geometry of the machine. A low built-in volume ratio implies higher flow rates and thus lower leakage loss. However, a too low built-in volume ratio would imply the under-expansion phenomenon, resulting in lower isentropic efficiencies. They also talked about the compromise between leakages and friction losses to determine the optimal rotational speed.
In 2007, Smith et al. [25] experimentally investigated a two-phase twin screw expander with "N" profiles in a TFC using R124 as the working fluid. The expander produced electric power of 22 kW with an isentropic efficiency of 0.74.
In 2014, Read et al. [26] performed a geometrical optimization of a twin-screw expander in a wet vapor Rankine cycle using water. The maximum isentropic efficiency obtained was 0.78 at nominal conditions. In 2016, Vasuthevan et al. [27] simulated a TFC operating with a two-phase twin screw expander and water. They assumed a sufficient heat transfer between vapor and liquid phases to reach a stable state within a time step. The simulations agreed with the experimental results. In 2018, Nikolov et al. [28] tried to minimize the internal leakages within the expander by investigating a water-injected twin-screw expander in a TFC. In 2020 Bianchi et al. [29] elaborated a numerical model of a TFC with R245fa as the working fluid. They varied the built-in ratio of the expander via a sliding valve in the casing. They showed that lowering the built-in volume ratio from 5.06 to 2.63 increased the volumetric efficiency increased from 0.53 to 0.77, whereas the isentropic efficiency decreased from 0.82 to 0.63 (due to under-expansion).

Another application for two-phase twin screw expanders was in the vapor compression refrigeration cycle as it could potentially improve the COP.
In 1997, Taniguchi et al. [30] introduce an innovative approach to replace the throttling process in vapor compression systems. The method involves harnessing power from the two-phase expansion process and utilizing it to directly recompress a portion of the vapor generated during expansion. These rotors rotate without the need for timing gear and operate within a process-lubricated, fully sealed unit termed an "expressor." Initial test results reveal that the overall efficiency of the expansion-compression process achieved by the expressor is approximately 0.55 (around 0.7 efficiency during the expansion phase and 0.8 efficiency during the compression phase. Brasz et al. [31] carried out experimental tests and showed that the "Expressor" had an isentropic efficiency of 0.66 when working with R113. They also showed that the rotor forces created by the compression and expansion processes can be partially balanced in order to eliminate the axial forces and reduce the radial bearing forces.

2.3 Application of two-phase expanders

This section presents different possible applications for two-phase expanders.

2.3.1 Vapor compression system

Refrigeration and air cooling systems are based on the vapor compression cycle (**Figure 2.4**). The cycle is composed of an evaporator, a vapor compressor, a condenser and of a throttling valve which can be replaced by a two-phase expander. [32]

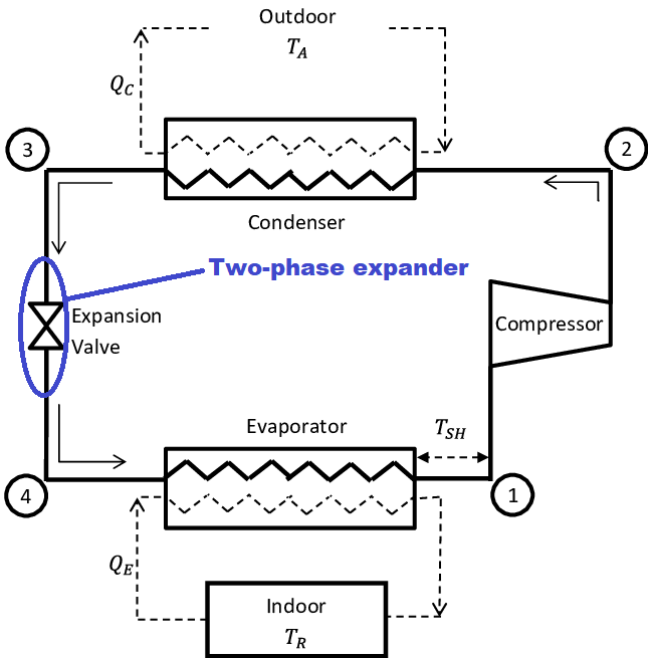

Figure 2.4: *Schematic diagram of vapor compression cycle. (source : [33])*

Replacing the throttling valve with a two-phase expander increases the COP of the cycle by: 1) Diminishing the electric power needed in the compressor by providing mechanical power with the two-phase expander; 2) Producing higher cooling power at the evaporator because of a lower specific enthalpy at the evaporator inlet (the irreversibilities in the two-phase expander are lower than in the throttling valve which allows keeping a higher specific enthalpy). In **Figure 2.5**, the evolution 3 $\rightarrow$ 4a represents the expansion in the throttling valve and 3 $\rightarrow$ 4b represents the expansion in the two-phase expander. One can see that the expansion with the two-phase expander creates less entropy than with the throttling valve.
A particular type of vapor compression refrigeration cycle is the transcritical one. The expansion takes place between the supercritical phase to the wet vapor phase.

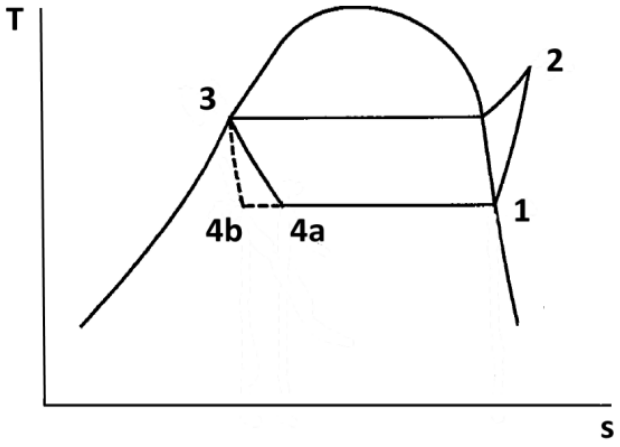

Figure 2.5: *Temperature-entropy diagram of a vapor compression cycle. (source : [32])*

2.3.2 Trilateral Flash Cycle (TFC)

Organic Rankine Cycles (ORC) are thermodynamical cycles that have the same structure as a Rankine cycle to produce power. Their difference remains in the fact that ORC uses refrigerant as working fluids instead of water (**Figure 2.6**). These refrigerants are more volatile than water and have lower critical temperatures, meaning that the refrigerant vaporizes at lower temperatures. This is particularly useful when working with heat sources coming from renewable energies as those heat sources have lower heating temperatures. The operating principle of the ORC is composed of four steps; the working fluid in the liquid state goes through a pump and gets a higher pressure, and then heat is supplied by the heat source through an evaporator to vaporize the fluid. After going through the evaporator, the working fluid goes through the expander where its enthalpy is reduced and converted into mechanical work at the shaft of the expander. Finally, the low-pressure fluid passes the condenser where its temperature decreases and is condensed to get a full liquid phase back.

With the increased demand for energy efficiency, research is being carried out to make ORCs more and more efficient. One of the proposed solutions is the Trilateral Flash Cycle (TFC). The TFC is a thermodynamical cycle suitable for low to medium heat sources. The components are the same as for the Rankine cycle which makes it a rather simple cycle. The main differences with the ORC are that the expansion is in the two-phase region and that the evaporator in the ORC no longer evaporates the fluid.
The following evolutions take place:

- $1 \rightarrow 2$: Heat supply at constant pressure until the liquid is saturated.
- $2 \rightarrow 3$: Two-phase expansion in the expander to generate power.
- $3 \rightarrow 4$: The gas-liquid working fluid is condensed completely.
- $4 \rightarrow 1$: The working fluid is pumped from low to high pressure.

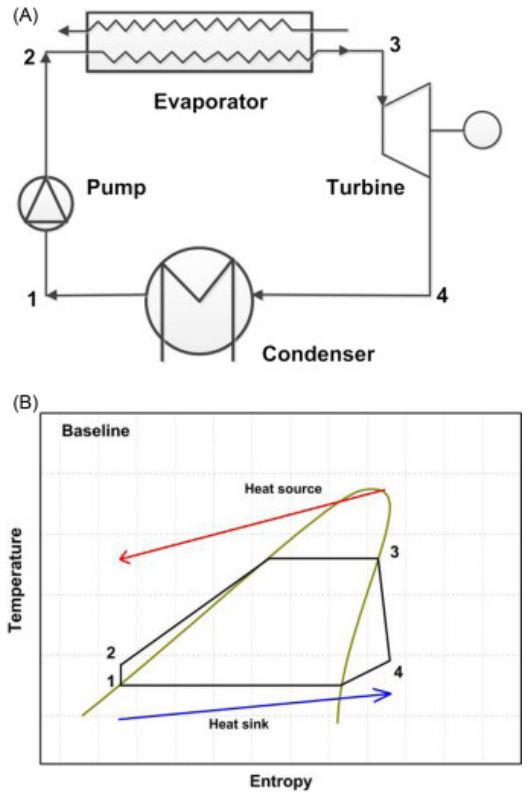

Figure 2.6: *(Above) Schematic layout of the component of an ORC (Under) Temperature entropy diagram of an ORC. (source : [32])*

Advantages:

- When receiving heat from a single-phase heat source, the working fluid doesn't evaporate which makes the cycle capable of very high heat recovery efficiency. The heat transfer is achieved with almost perfect temperature matching and irreversibilities are therefore minimized. The low thermal irreversibility implies a higher cycle thermodynamic efficiency.
- Since higher temperatures at the expander's outlet are reached, higher power outputs can be produced by the expander (by nearly 50% compared to the ORC).

Disadvantages:

- TFC requires a greater feed pump power since a higher flow rate is necessary to have the same power output as the one produced with an ORC. This is due to the lower energy input from the low temperature heat source.
- As stated previously, not a lot of literature is available on two-phase expansion processes and it stays a rather new and unknown process.
- It is crucial to use fluids with critical temperatures close to the maximum temperature of the cycle to increase the density of the saturated vapor resulting from the flash stage.

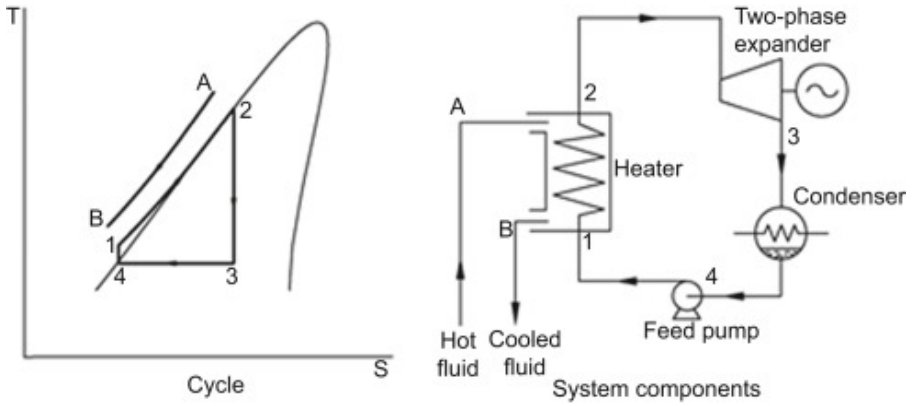

Figure 2.7: *(Right) Schematic layout of the component of a TFC cycle (Left) Temperature entropy diagram of a TFC. (source :[34])*

- Compared to conventional Rankine cycles, the heat exchangers are larger due to the greater heat transfer and the increased area resulting from closing temperature matching between the working fluid and the heating source.

In the case of a higher-temperature heat source (180-210°C), the volume ratio to be realized over one stage of the two-phase expander might be too large and a second stage might be necessary. This second stage could be too large to be cost-effective or beyond current manufacturing limits. To solve this problem, the Smith cycle (**Figure 2.8**) was proposed. In this cycle, the first stage of the expansion takes place in a two-phase expander ($2 \rightarrow 3$). At the end of the first expansion (point 3) the working fluid is separated into two flows; the saturated liquid phase (point 3') and the dry saturated vapor phase. The dry saturated vapor phase goes through a second expansion process in a single-phase expander ($3 \rightarrow 3$").

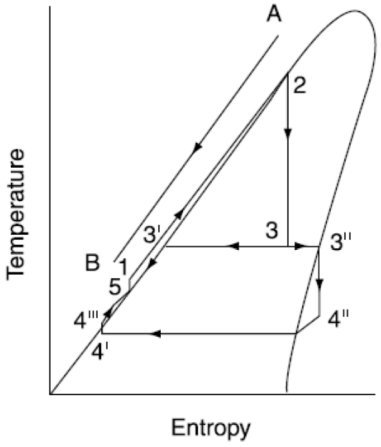

Figure 2.8: *Temperature-entropy diagram of the Smith cycle (source :[32])*

2.3.3 Wet vapour ORC

Another application for the two-phase expander is the wet vapor ORC. In this cycle, the expansion begins in the two-phase region and ends in the two-phase region, in the superheated region or on the saturated line (**Figure 2.9**). The evaporation temperature can be higher than the critical temperature. More heat can be collected in wet vapor ORC compared to ORC as the evaporation temperature can be higher with the same input thermal power. It implies a bigger heat input which leads to a greater electric power per unit of mass flow rate and a higher cycle thermodynamic efficiency. The vapor quality at the expander inlet can be controlled to partially match the temperatures of a particular heat source. This can make the wet vapor ORC more flexible than TFC.

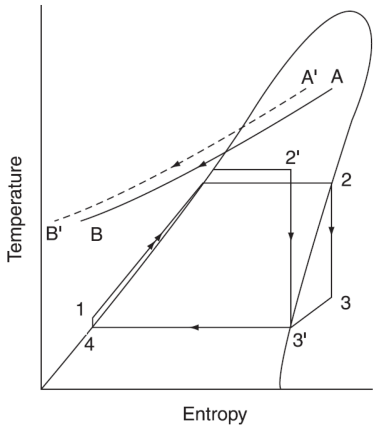

Figure 2.9: *Temperature-entropy diagram of a traditional ORC (1-2-3-3'-4) and wet vapor ORC (1-2'-3'-4) (source :[32])*

Chapter 3

Test bench description

To realize the two-phase expansion process of the REGEN-BY-2 cycle with HFO R1233zde, a two-phase ORC is implemented into a test rig to test a commercial scroll expander. The test bench is also able to carry out experiments outside the conditions necessary for testing the expansion of the REGEN-BY-2 cycle. The test rig is located in the thermodynamics and transport phenomena laboratory of the National Technical University of Athens. This test rig is represented in **Figure 3.1**. As already stated in Section 1.1.2, the expansion tested is between points 7 and 8 of the REGEN-BY-TWO cycle. The thermodynamic points are reminded in **Table 3.1**.

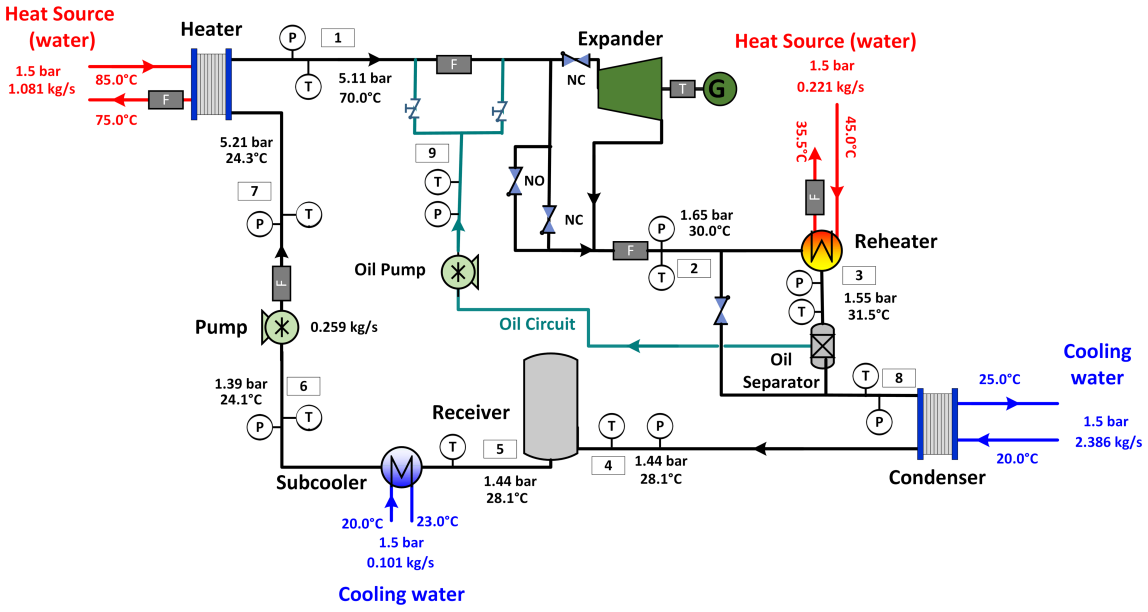

Figure 3.1: *Configuration and nominal operational conditions of the two-phase ORC test rig. Measuring devices: P: Pressure Transducer, T: Temperature sensor, F: Coriolis flow meter. NO and NC refers to Normally Open and Normally Closed solenoid valves. All other depicted valves are manual ball valves.*

Table 3.1: *Points necessary for the two-phase expansion of the REGEN-BY-2 cycle tested.*

Points	Pressure [bar]	Vapour quality [-]
1	5.4	0.713
2	1.6	0.822

In **Figure 3.2**, the pressure-enthalpy diagram of the two-phase ORC is represented. The following evolution takes place: 1→2 Expansion; 2→2a Superheating; 2a→3 Condensation; 4→5 Sub-cooling; 5→6 Pumping; 6→1 Partial Evaporation. The nominal circulating mass flow rate of the refrigerant is 0.26 kg/s.

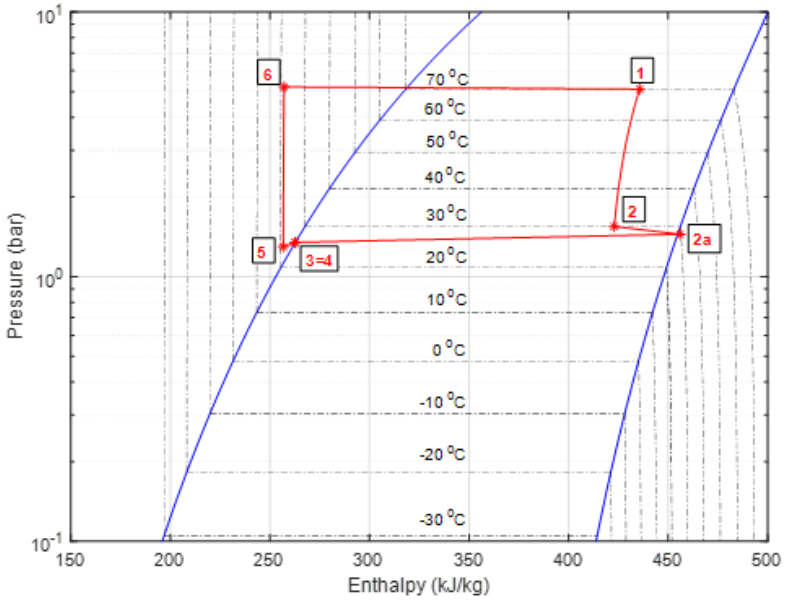

Figure 3.2: *Pressure-Enthalpy diagram of the two-phase ORC cycle with R1233zde.*

To assure the good functioning of the test rig, some important points must be taken into consideration:

- In the ORC cycle, the pump is often under cavitations. A sub-cooler at the pump inlet has been implemented in order to ensure a cavitation-free operation.
- To ensure the good functioning of the expander, the refrigerant needs to be charged with oil. In the tests carried out in this thesis, 10% of the total refrigerant/oil mixture mass is oil. However, the exact Oil Circulation Ratio (OCR) provided to the expander at each moment is not known. Indeed, oil traps can exist and be amplified or not depending on the mass flow rate.

3.1 ORC components

This section describes the different components used in the test bench. The test bench is mounted on steel frames. The refrigerant is flowing through standard refrigerant copper pipes. To minimize the pressure drops in the pipes between [200-400] mbar, the pipes need to respect dimensioning criteria. Those criteria depend on the state of the refrigerant at nominal conditions. Indeed, for the same flow rate, when the refrigerant is in the vapor phase or the two-phase, the density is lower than in the liquid phase. This means that the velocity of the fluid increases and thus the pressure losses too. The fluid velocity can be decreased by increasing the hydraulic diameters of the pipes. For vapor and two-phase flows the velocity of the flow had to be in the range of 10-2 5m/s and for liquid flows the velocity should be less than 2 m/s. This ensures low-pressure drops and sufficiently low speeds to enhance the homogeneity of two-phase refrigerant and oil mixtures.

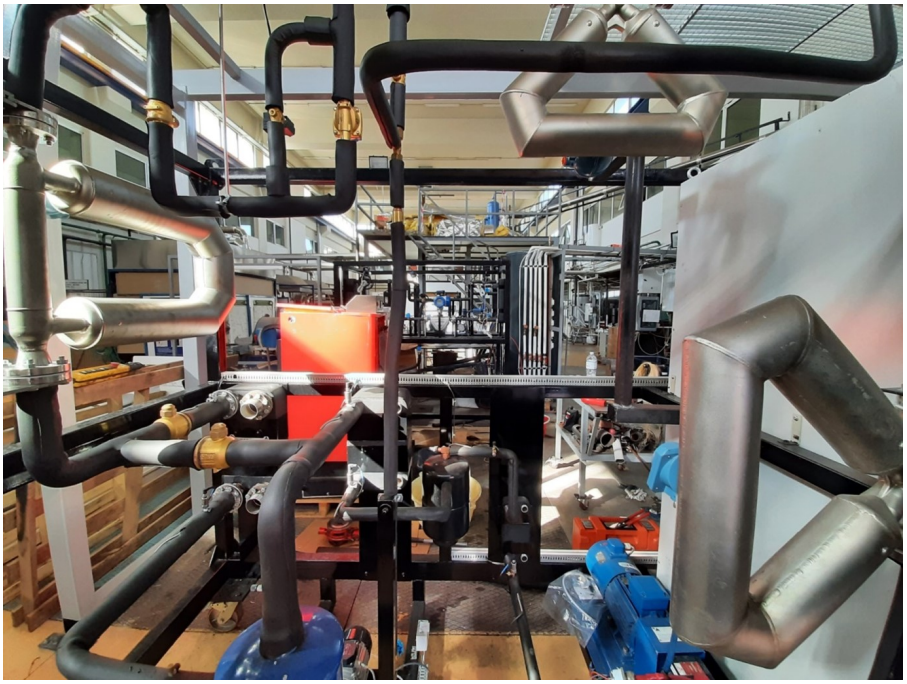

Figure 3.3: *Picture of the Two-phase ORC at the NTUA lab.*

3.1.1 ORC pump

As in most ORC cycles, a positive displacement pump has been selected. The pump selected is a Neoprene diaphragm pump and is compatible with R1233zde. The pump is driven by a 4-pole asynchronous electrical motor (3kW rated power – 1500rpm@50Hz). The pump characteristics are available in **Table 3.2**.

Table 3.2: *Pump characteristics.*

Model	Hydracell G10-X
Max. flow rate	33.4 l/min
Max. pressure	17 bar
Max. temperature	60°C

The mass flow rate is linearly adjusted by controlling the rotational speed of the motor and thus of the pump. The rotational speed is controlled via a Variable Frequency Drive (VFD) which ensures a flexible operation of the test rig. The VFD is a Siemens Sinamics V20 with 3kW of rated power.

3.1.2 Expander/Generator

The expander used in the cycle is a modified scroll compressor by the partner EXOES and is used as an expander. The commercial machine selected for the test is a compressor coming from car Heating, Cooling and Air-Conditioning (HVAC) systems. The compressor displacement can be reduced by 39% via a reduction port if the built-in volume ratio needs to be reduced. In this application, the displacement is sealed and the expander can thus be considered as a single-stage expander with the maximum displacement possible. The expander characteristics are showed in **Table 3.3**.

Table 3.3: *Expander characteristics.*

Model	SANDEN TGVE08
Swept volume	86.22 cc/rev
Built-in ratio	2.3
Max. speed	6000 rpm
OCR	Min. 5%

The expander is coupled to an asynchronous 2-pole motor/generator (4kW rated power, 3000rpm @50Hz – 3600rpm @60Hz) via a pulley belt system with a transmission ratio of 1.7, ensuring a maximum rotational speed of 6100 rpm at the expander (3600*1.7). The rotational speed of the motor/generator is controlled via a VFD (Siemens Sinamics G120, 5.5kW). The motor mode is activated at the start-up of the tests to give the expander a rotational speed without any pressure change. The solenoid valve at the expander inlet is closed and the expander is bypassed. Once the expander is at the wanted speed, the flow can be directed via the solenoid valves to the expander to produce mechanical power (generator mode) at the same rotational speed. The produced electrical power is in this case fed back to the grid.

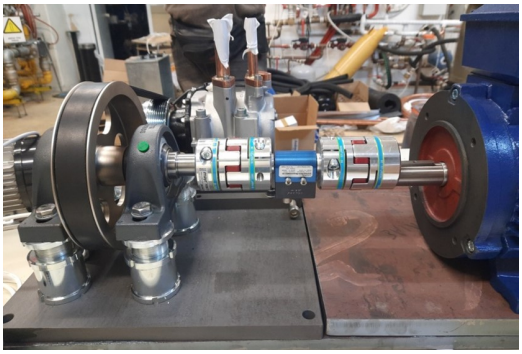

Figure 3.4: *The commercial SANDEN expander coupled via a belt-pulley system to an asynchronous motor/generator which is driven by a regenerative VFD.*

3.1.3 Heat exchangers

The heat exchangers (HEX) used in the cycle were ordered from SWEP and are plate exchangers. The characteristics are summarised in **Table 3.4**.

Table 3.4: *HEX characteristics.*

HEX	Model	No. Plates	HEX area ($\%$ over-surfacing)	Capacity	ΔP Refrigerant
Evaporator	B120TH	30	3.70 m^2 (53$\%$)	46kW	93.5 mbar
Superheater	B320LTL	30	3.47 m^2 (33$\%$)	8.6kW	102 mbar
Condenser	B35TH0	62	5.64 m^2 (21$\%$)	49.7kW	51 mbar
Subcooler	B10TH	10	0.25 m^2(66$\%$)	1.25kW	73.6 mbar

3.2 Oil Loop

In ORC systems, the usual practice is to charge the refrigerant with oil up to 5-8$\%$ of the total refrigerant mass. The mixture is then used as the working fluid and provides lubrication to the expander. The exact amount of oil provided to the expander at each moment is not known. The selected oil is the POE oil Emkarate RL 32MAF.

As stated in section 3.2.1, the presence of oil in the heat exchangers and the pump is not desirable, thus an oil loop is implemented to try and separate the oil from the refrigerant and make it circulates only in the expander. The oil circuit works in the following way:

- After the expansion, the mixture's temperature is increased with a reheater to have a superheated state. Indeed, to separate the oil from the refrigerant in an oil separator, no refrigerant can be trapped in the oil. There is the possibility to bypass the reheater and the oil separator if the oil content is low (below 8 $\%$ mass).

- After the reheater, the mixture goes through the oil separator whose working principle is explained in section 3.2.2.
- The oil is pumped by the oil pump and is directed at the expander inlet. It can be led either before or after the Coriolis flow meter to take the oil or not into account in the post-processing.

In the experiments carried out for this thesis, the oil circuit is bypassed because they were too many losses at the pump during the essays. The oil content is of 10% mass.

3.2.1 Impact of the presence of oil in the refrigerant

Volumetric expanders such as scroll expanders are usually lubricated to limit internal leakage, decrease friction losses, and have a longer lifetime. The oil also provides cooling.

The presence of oil in the refrigerant leads to several drawbacks in the ORC; it decreases the heat transfer coefficient in the two-phase heat exchangers, it changes the flow configuration, it increases the pressure drops in the heat exchangers and it modifies the thermodynamical equilibrium and properties of the refrigerant. The COP decreases when increasing the oil circulation ratio [35].

The evaporator is the most penalized component by the presence of oil [36]. Over the evaporation, the refrigerant evaporates while the oil doesn't (the boiling temperature of the oil is much higher than the one of the refrigerant), so the liquid phase becomes more and more concentrated in oil. The viscosity of the oil is much bigger than the viscosity of the refrigerant, thus, the viscosity of the mixture increases. Due to this phenomenon, there is an accumulation of oil at the evaporator. This circulation is at the origin of a deviation from theoretical behavior and without taking the oil into consideration, the heat balances around the evaporator do not add up.

3.2.2 Oil separator

The separator is used to separate the liquid (primarily oil) from the vapor phase (refrigerant). A patented design of a helical type oil separator that ensures high efficiency and low-pressure drop from HENRY Technologies (Henry S-5188-CE with a maximum volume flow rate of 13.6 m^3/h) was selected for this test rig. The oil separator is combined with an oil reservoir for compactness. The oil from the reservoir is at low pressure and needs to be pumped to be fed to the expander at a higher pressure and specific mass flow rate.

Figure 3.5: *The selected helical type oil separator/reservoir*

3.2.3 Oil pump

The pump selected to pump the oil from the reservoir to the inlet of the expander is a gear pump driven by a VFD. In the same way as the ORC pump, the oil mass flow rate is proportional to its rotational speed.

3.3 Measuring Equipments

3.3.1 Temperature sensors

The temperature of the refrigerant in the cycle is measured via Standard Resistive Temperature Detectors (RTD) Pt-100. In this kind of temperature sensor, the temperature is measured based on the resistance change induced by the temperature. Their main advantage is that they are stable over long periods of time and are accurate. The class of the sensor is A which means that the accuracy expected is more or less of 0.1°C. The range of operating temperature is between -200°C and 850°C. The sensors are placed in direct contact with the refrigerant.

3.3.2 Pressure sensors

The pressure of the refrigerant is measured throughout the cycle with pressure transducters.

Table 3.5: *Pressure transducters characteristics.*

Side	Model	Pressure range	Current signal	Accuracy
High-pressure	Emerson PT5-07	[-0.8 - 7] bar	[4-20] mA	$\pm$ 1 % Full Scale
Low pressure	Emerson PT5-18	[0 - 18] bar	[4-20] mA	$\pm$ 1 % Full Scale

3.3.3 Safety pressostats (pressure switches)

Safety pressostats have been installed in the ORC circuit at the low and high-pressure sides. The pressure switches automatically stop the operation of the VFD of the pump to avoid damage to the rig due to too high pressure or to avoid damaging the pump itself due to too low pressure.

3.3.4 Torquemeter

The torque at the shaft of the expander is measured via a torquemeter. The torquemeter used in this test rig is a shaft-type torque transducer.

Table 3.6: *Torque transducters characteristics.*

Model	Output signal	range	Accuracy
Interface T4	± 5V	0-10Nm	0.1% combined error

3.3.5 Coriolis flow meters

A first Coriolis flow meter to measure the mass flow rate of the ORC cycle is installed at the pump outlet. To measure the density at the outlet and at the inlet of the expander two Coriolis flow and density meters are installed. Those flow meters have a low tube frequency which makes them perfect for two-phase flow. The main characteristics are depicted in **Table 3.7**.

Table 3.7: *Coriolis flow and density meters characteristics.*

Model	Micromotion Elite Series
Density accuracy	± 0.2 kg/m^3
Density repeatability	± 0.1 kg/m^3

The Coriolis flow and density meters measures the mass flow rate and the density based on the Coriolis effect.

To avoid the occurrence of supersonic gaseous flow in the inner tubes of the flow meter, the **Equation 3.1** provided by the manufacturer, for the design conditions of the test rig, must be checked. The tube diameter of the flow meter model is then chosen.

$$\dot{m}_{gas} = 2 \cdot M \cdot \rho_{gas} \cdot \frac{\pi \cdot D^2}{4} \tag{3.1}$$

Where $\dot{m}_{gas}$ is the measured mass flow rate, M is the Mach number, ρ_{gas} is the density of the fluid. The Mach number is worth 0.2 for calculating the nominal mass flow rate and 0.3 to determine the upper limit. The models are chosen based on this equation and are available in **Table 3.8**

Table 3.8: *Chosen Coriolis models.*

Model	Location	Diameter Nominal (mm)
CMF100	Expander inlet	25
CMF200	Expander outlet	50

Figure 3.6: *The installed CMF200 Coriolis flow and density meter of Emerson Micromotion Elite series.*

3.3.6 Electromagnetic water flow meters

In the hydraulic circuit of the NTUA laboratory, ultrasonic flowmeters are installed and allow to measure the mass flow rates of the water coming in the heat exchangers of the ORC. However, the calibration of the density measured by the Coriolis at the expander inlet is made via the heat balance on the evaporator (Section 3.3.7) and their precision are not high enough for that purpose. Two higher precision electromagnetic flow meters are thus installed at the evaporator outlet and at the reheater outlet. The characteristics of the flowmeters are in **Table 3.9**.

Table 3.9: *Water flow meters.*

Model	Location	Accuracy	Repeatability
Ultrasonic flowmeters	Condenser and Subcooler	2%	-
KROHNE OPTIFLUX 1000	Evaporator and Reheater	$<$1%	$\pm$0.1% of MV

Figure 3.7: *The selected electromagnetic water flow meters by KROHNE.*

3.3.7 Density and vapor quality measurement

To determine the vapor quality and the properties of the mixture at the expander inlet, the Coriolis flowmeter is used. It does not provide an accurate measure of the mass flow rate in the two-phase region, however, it also measures the density, which, after a linear calibration, can be used to give a direct estimation of the quality at the inlet of the expander.

To calibrate the density measured by the Coriolis, the heat balance on the evaporator is used. Indeed, the density at the expander inlet can also be determined from that heat balance as described by the following equations (considering negligible heat losses in the heat exchanger and the pipes):

$$\dot{m}_w \cdot C_{p,w} \cdot (T_{w,in} - T_{w,out}) = \dot{m}_{ORC} \cdot (h_{out,ev} - h_{in,ev}) \tag{3.2}$$

where $h_{out,ev}$ is the enthalpy of the two-phase flow mixture at the evaporator inlet, $h_{in,ev}$ is the enthalpy of the mixture at the evaporator inlet, $T_{w,out}$ and $T_{w,in}$ are the outlet/inlet temperatures of the water, $C_{p,w}$ is the specific heat capacity of the water under constant pressure at the average water temperature, and $\dot{m}_w$ and $\dot{m}_{ORC}$ the mass flow rates of the water and the mixture respectively.
From **Equation 3.2**, $h_{out,ev}$ can be determined, and from that and the measured pressure, the density can be determined.
The density determined with the heat balance at the evaporator is then used to calibrate the density measured by the Coriolis flowmeter. The parameters of the linear correlation are determined using a standard least squares linear regression model.

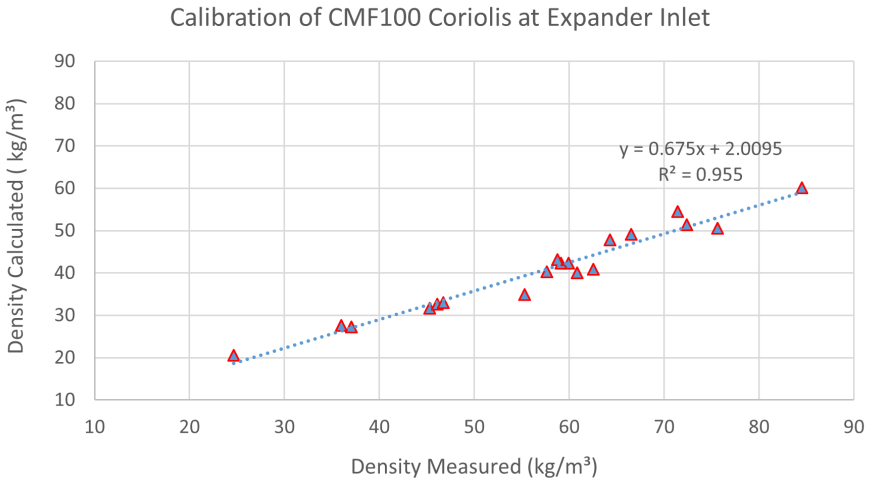

Figure 3.8: *Linear regression for the calibration of density measurements of the Coriolis flowmeter at two-phase conditions using the calculated density from the heat balance in the evaporator HEX.*

As the inlet temperature of the water is heated by a boiler, its value oscillates. Due to latency, the heat balance on the waterside and the refrigerant side is not always matching. Complicated stable conditions were only obtained for the calibration of the Coriolis flowmeter. The density measured by the Coriolis is the density of the oil-refrigerant mixture and the oil contribution is removed to get the density of the refrigerant. The density of the refrigerant deduced from the calibration is used to determine the enthalpy at the expander inlet, which is then used to calculate the vapor quality with **Equation 3.3** for all the experimental tests.

$$Q = \frac{h_{r,in,exp} - h_{liq}}{h_{vap} - h_{liq}} \tag{3.3}$$

where $h_{r,in,exp}$ is the enthalpy of the refrigerant at the expander inlet. h_{liq} and h_{vap} are the enthalpies of the saturated liquid and the saturated vapor respectively.

3.4 Hydraulic loop

The hydraulic circuit is used to provide heat sources to the partial evaporator and the superheater of the ORC loop and to serve as a heat sink to the condenser and the sub-cooler. The hydraulic circuit is implemented in the Laboratory of Steam Boilers and Thermal Plants (LSBTP) in NTUA. It is a circuit that can provide and dissipate heat at different temperatures and flow rates with flexibility and accuracy and that also can be connected to several test benches of the laboratory. To be able to supply heat at different temperatures and flow rates required for this ORC, the hydraulic infrastructure of the laboratory has been modified and expanded.

This circuit is composed of four storage tanks at three different levels of temperature. The high-temperature storage is at 90°C and is supplied by a 90kWth gas boiler; the two medium-temperature storage tanks have temperatures between 20 and 40°C and their heat is dissipated through an intermediate HEX to a large external tank which is cooled down by a cooling tower situated outside of the lab. Finally, the low-temperature storage tank's temperature is between 5 and 15°C and is cooled by an air-cooled chiller.
To achieve temperature control, the high- and medium-temperature tanks are mixed for the heat supply needed at the evaporator and the reheater. The medium- and low-temperature tanks are mixed for the cooling needed in the condenser and the sub-cooler. Regarding flow rate control, Pressure-Independent Balancing Control Valves (PIBCV) have been installed in each branch of both the hot and cold sides. Regarding flow rate control, Pressure-Independent Balancing Control Valves (PIBCV) have been installed to control the water mass flow rates. The hydraulic system is controlled by an Industrial DDC Controller (Schneider Electric) monitored through a dedicated Graphic User Interface (**Figure 3.9**).

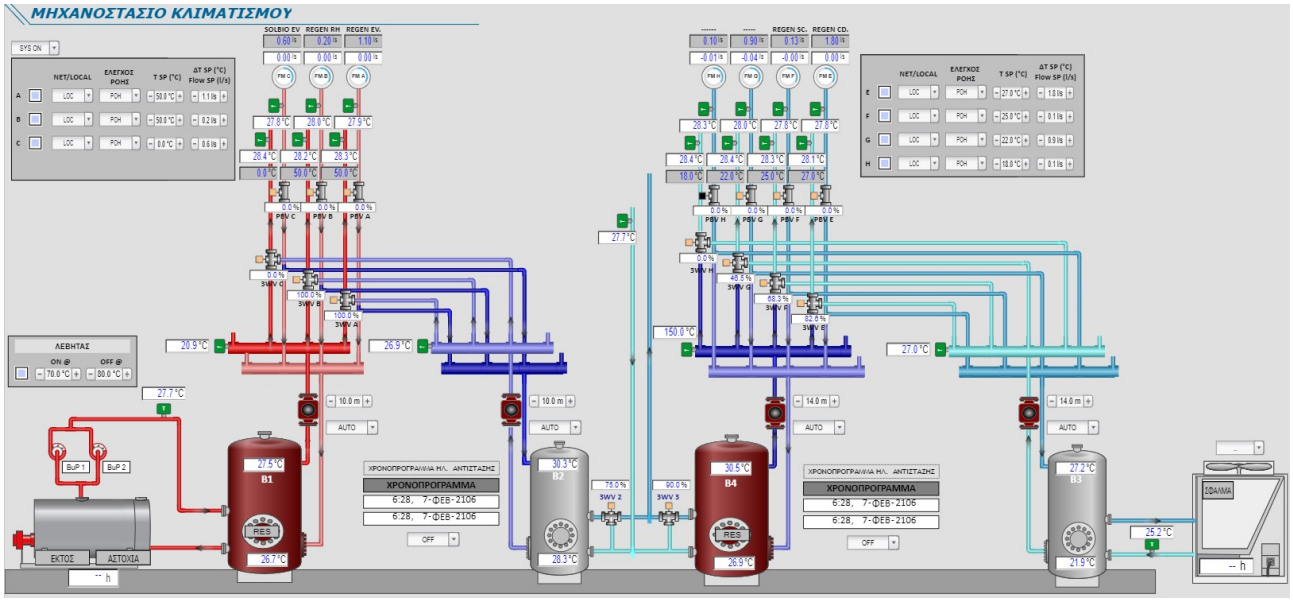

Figure 3.9: *Graphic User Interface of the controller of the hydraulic setup at the LSBTP laboratory in NTUA.*

3.5 Control and monitoring of the test bench

An electrical cabinet includes all the required hardware for the safe and reliable operation of the setup. The cabinet has all the required safety devices (Circuit Breakers, Residual Current Devices etc), the Variable Frequency Drives (VFD) for the expander, the ORC pump and the

Oil pump. The high and low pressure switches installed on the inlet and outlet of the ORC pump are directly connected to the VFDs, stopping immediately their operation in case of fault detection. An emergency stop button directly cuts the power supply of the whole cabinet.

The acquisition system comprises I/O cards that read analog and digital signals from the sensors and transmit analog output to the actuators. The I/O cards are internally communicating with the controller using the EtherCat protocol. Apart from the physical signals, also various variables are monitored from the VFDs, the Power Meters, and the Coriolis Flow Meters through a local Modbus RTU fieldbus. Regarding the control part, an industrial PC from Advantech (AMAX-5580) controls the whole setup. The LabView software is used to display and record the data sent from the acquisition chain. In LabView, the signals from each sensor are converted into physical value by scaling them. Physical values from each sensor are averaged and recorded every second. The Graphic User Interface (GUI) is depicted in **Figure 3.10**.

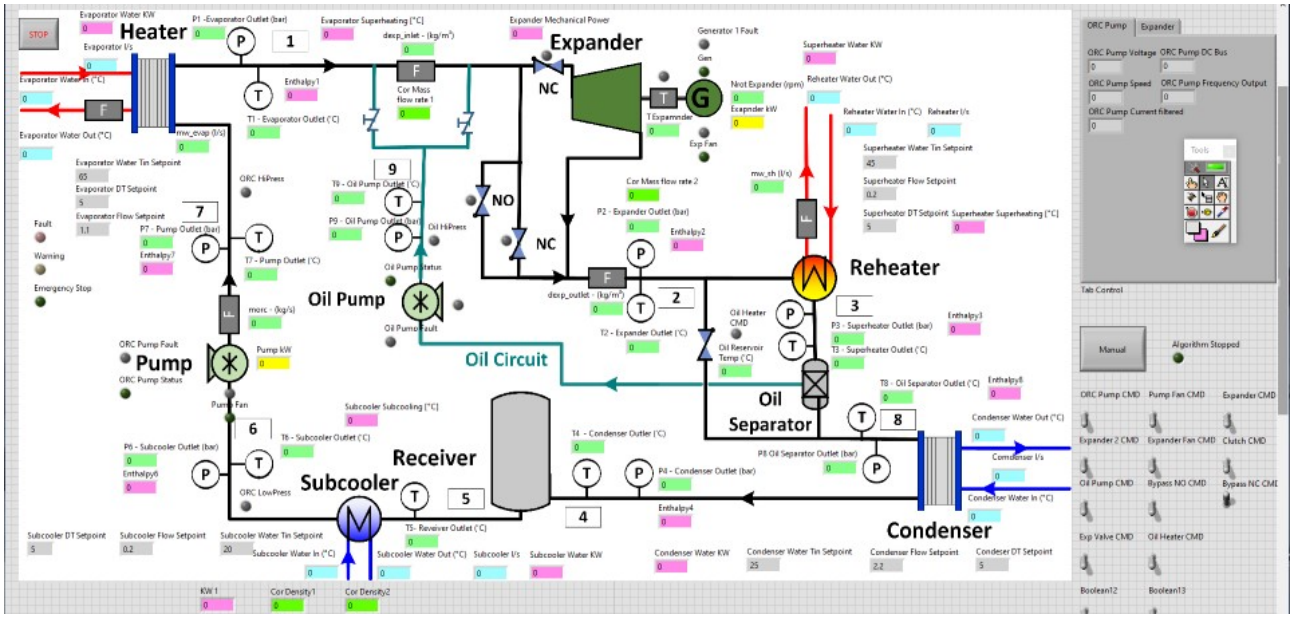

Figure 3.10: *Monitoring Graphic User Interface of the two-phase ORC test-rig at the LSBTP laboratory in NTUA.*

Chapter 4

Experimental investigation

4.1 Experimental campaign

The experimental campaign was conducted over 3 weeks and a total of 49 experimental points were recorded. A test starts by stabilizing the test bench for a point in the one-phase region at the expander inlet. This first point is usually hard to stabilize, but once it is done, the other experimental points are recorded more or less every 10 to 15 minutes. This time allows an increase of the water temperature at the evaporator inlet (until around 80°C) and then a decrease (around 75°C) that corresponds to a turn on and off of the boiler. The goal of the tests is to characterize the commercial expander, especially in the two-phase region. As explained in Section 1.1.2, the scroll expander also has to be tested for the expansion '7→ 8' of the REGEN-BY-TWO cycle. To characterize the expander, the main operational parameter that affects its performance and efficiency (measured by the isentropic and volumetric efficiency respectively) are varied and listed in **Table 4.1** as well as their range of operation.

Table 4.1: *Test range of the experiments*

Vapor quality at the expander inlet	0.5-1
Expander speed	1700-3200 RPM
Pressure ratio of the expander	1.8-2.4
Pressure at the expander inlet	6 bar

Section 4.3 explains the two different kinds of experimental tests that have been carried out to test those ranges of operation.

4.1.1 Start-up procedure

The start-up procedures is composed of the following steps:

1. The flow is first driven through the two open by-pass valves and the valve at the expander inlet remains close to prevent the flow to go through the expander. The pump speed is slowly increased as well as the inlet water temperature of the evaporator. Once the temperatures of the ORC have caught up, the system is stabilized (in terms of vapor quality, mass flow rate, cycle pressures and temperatures).
2. The generator is turned on at a low fixed speed as a motor.
3. Then the valve at the expander inlet is opened and the scroll clutch is enabled simultaneously.
4. The two bypass solenoid valves are closed.
5. The expander speed is increased until reaching the desired (pre-calculated) operational points.
6. The main system operational parameters are then stabilized.
7. The water flow rates in the HEXs, the pump and/or expander speeds are adjusted to achieve the desired conditions.

The opposite procedure is followed to disengage the scroll expander from the system.

4.1.2 Control of the test-bench in steady-state conditions

To control the bench, several actuators are available. They are cited in **Table 4.2** as well as their direct and indirect effects on the system.

The main operational parameters that affect the expander's performance and efficiency are the vapor quality at the expander inlet, the expander rotational speed, the pressure ratio and the expander inlet pressure. These parameters are modified in the following ways;

- **The expander inlet pressure:** at constant rotational speeds of the expander and the pump, the inlet pressure changes mostly with the inlet water temperature of the evaporator. The hot water mass flow rate is used to fine-tune the inlet pressure. In superheated conditions, the inlet pressure can be fine-tuned by adjusting the expander rotational speed: an increase in the expander speed reduces the inlet pressure and vice versa.
- **The expander inlet vapor quality:** At constant rotational speeds of the expander and constant inlet pressure, the vapour quality is changed by varying the ORC pump speed and thus changing the refrigerant-oil mixture mass flow rate. Increasing the mass flow rate decreases the enthalpy at the evaporator outlet/expander inlet which also decreases the vapour quality.

- **The pressure ratio:** It is changed by varying the outlet pressure of the expander (the inlet pressure of the condenser). This pressure is exclusively imposed by the inlet water conditions in the condenser. At constant inlet pressure of the expander, various pressure ratios may be achieved by varying the cold water temperature/flow in the condenser.

Table 4.2: *System actuators and their effect on the system.*

Actuators	Direct effects	Indirect effects
Hot water temperature at the evaporator inlet	Evaporation temperature, Expander inlet pressure	Expander inlet density, Expander shaft work
ORC pump rotational speed	Refrigerant/oil mixture mass flow rate	Expander inlet vapor quality at constant expander rotational speed and evaporation/condensation temperature, Expander shaft work
Expander rotational speed	Expander inlet pressure at superheated conditions, Expander inlet vapor quality at constant evaporation/condensation temperature ORC pump rotational speed	Expander inlet density, Expander shaft work
Cold water temperature and/or mass flow rate	Condensation temperature, Expander outlet pressure	Pressure ratio, Expander shaft work

4.2 Post-processing

4.2.1 Experimental points identifications

Each test campaign is recorded in LABVIEW providing an Excel file containing all of the sensor measurements. Every 2 seconds, the sensor measurements are registered. The recorded data are then post-processed through a MATLAB code. One Excel file contains several experimental points, the first step of the post-processing is thus to identify those experimental points.

Before identifying the experimental points, the steady-state points are singled out. A point is considered as steady-state when 20 recorded points in a row respect certain criteria. The criteria to verify the steadiness of the experimental points are:

- The pump and expander speed set must be constant.

- The variation of the expander inlet pressure must stay below 2% and the variation of the outlet pressure must stay below 2.5%.
- To verify the stability of the boiler, the inlet and outlet temperatures of the evaporator are checked, with a maximum variation of 2.5 % for both measures. The heat capacity of the evaporator is also checked and its variation must stay below 5 %.

After the identification of the steady-state points, the experimental points need to be singled out. One experimental point is the mean value of several steady-state points.

4.2.2 Data reduction

Once the experimental points are identified, those values go through a data reduction process to calculate the performances of the expander.

Assumptions

The data reduction of the sensor measurements is based on several assumptions:

- No refrigerant is present in the oil, and the properties of the oil-refrigerant mixture are thus simply the addition of the properties of the pure components.
- There is a thermodynamic equilibrium at the expander inlet. This assumption means that the vapor and the liquid phase have the same temperature and the same pressure.

Oil properties

Taking into account the oil properties in the evaluation of the expander's performance is essential in order to have more realistic performances. The oil (POE 32) is considered incompressible and its properties are calculated as a function of the temperature using the following equations: (Dickes, 2019 [37])

$$\rho_{\text{oil}} = a_0 + a_1 \cdot T \qquad C_{p,\text{oil}} = a_2 + a_3 \cdot T \tag{4.1}$$

$$h_{oil} = \int_{T_0}^{T} C_{p,oil}\, dT \quad s_{oil} = \int_{T_0}^{T} \frac{C_{p,oil}}{T}\, dT \tag{4.2}$$

where $a_0 = 996$, $a_1 = 0.7547$, $a_2 = 1158.2$ and $a_3 = 2.3639$ and at the reference temperature $T_0 = 273.15K$, $s_{oil} = s_r$ and $h_{oil} = h_r$.

Thermodynamic model of the mixture properties

To determine the properties of the oil-refrigerant mixture, the properties of the oil are simply added to the properties of the refrigerant. This method is a simplification because, in reality,

a part of the refrigerant is always trapped in the oil. In the explanation of the semi-empirical model with oil (Section 5.2), a more accurate model is described. However for simplicity, in the post-processing, a simple addition is made.

The calculation of any properties (represented by the variable X) is made with **Equation 4.3**.

$$X_{mix} = (1 - OCR) \cdot X_r + OCR \cdot X_{oil}(T) \tag{4.3}$$

where X_{mix} represents any property of the oil-refrigerant mixture, $OCR = \frac{m_{oil}}{m_{tot}} = \frac{m_{oil}}{m_r + m_{oil}}$ is the Oil Circulation Ratio, X_r represents the refrigerant properties and X_{oil} represents the oil properties.

Expander performance evaluation

Vapour quality at the expander's entrance:
As explained previously, the vapor quality at the expander inlet is determined based on the density measured by the Coriolis flowmeter (Section 3.3.7). The vapor quality is determined only based on the refrigerant:

$$Q_1 = \frac{h_{1,r}(P_1, \rho_{1,r}) - h^{\sigma}_{liq}(P_1)}{h^{\sigma}_{vap}(P_1) - h^{\sigma}_{liq}(P_1)} \tag{4.4}$$

Where "1" represents the state at the expander inlet. The subscripts *Vap* and *Liq* represent the vapor and liquid phase while σ represents the saturated state. $h_{1,r}(P_1, \rho_{1,r})$ is the enthalpy determined based on the density measured by the Coriolis.

Isentropic efficiency:
To determine the isentropic efficiency, the isentropic enthalpy at the expander's outlet needs to be calculated. To do so, the entropy of the mixture is conserved and the isentropic properties can be determined based on this conservation **Equation 4.6**.

$$s_1 = (1 - OCR) \cdot s_{1,r} + OCR \cdot s_{1,oil} \tag{4.5}$$

$$s_2^{is} = s_1 \tag{4.6}$$

Where "2" represents the state at the expander outlet and *is* represents the isentropic state. Only the entropy of the mixture is known, which means that the isentropic enthalpy cannot directly be guessed from it with CoolProp and an iterative procedure needs to be applied. The iterative method chosen is the bisection for its simplicity and its robustness. At each iteration, the entropy $s^{is}_{2,r}(k)$ (if k, the iterative process step number, then for the first step k=1) and the isentropic temperature $T_2^{is}(k)$ are determined based on the guess on the enthalpy $h^{is}_{2,r}(k)$ and the expander outlet pressure (P_2 that is measured). Since $T_2^{is}(k)$ is known, the isentropic

thermodynamic properties of the oil can also be calculated.
The entropy of the oil refrigerant mixture at step k can be explicitly calculated as

$$s_2^{is}(k) = s_{2,r}^{is}(k) \cdot (1 - OCR) + s_{2,oil}(k) \cdot OCR \tag{4.7}$$

The convergent target of the bisection is:

$$s_1 - s_2^{is} < \epsilon \tag{4.8}$$

where $\epsilon = 1^{-10}$. Once the solver has converged, the isentropic state 2^{is} is considered as known and the isentropic efficiency of the expander can be calculated.

The shaft work is calculated:

$$\dot{W}_{sh} = T_{gen} \cdot N_{gen} \cdot \frac{\pi}{30} \cdot \frac{1}{\eta_m} \tag{4.9}$$

where T_{gen} is the measured shaft torque, N_{gen} is the imposed rotational speed on the expander. η_m is the mechanical efficiency, assumed equal to 0.9, and represents the transmission losses of the belt and pulley system.
And the isentropic efficiency is defined as in **Equation 4.10**.

$$\epsilon_{is} = \frac{\dot{W}_{shaft}}{\dot{m}_{ORC} \cdot (h_1 - h_{2,is})} \tag{4.10}$$

where $\dot{m}_{ORC}$ is the mass flow rate of the mixture. In this definition, the oil-refrigerant mixture is supposed to have an isentropic interaction.

Volumetric efficiency:
Concerning the volumetric efficiency, it is determined as such;

$$\varepsilon_v = \frac{\dot{m_{th}}}{\dot{m_{ORC}}} \tag{4.11}$$

Where the theoretical mass flow rate is worth:

$$\dot{m}_{th} = \frac{V_{dis}}{r_{v,in}} \cdot \frac{N_{exp,RPM}}{60} \cdot \rho_{1,cali} \tag{4.12}$$

Where the $\rho_{1,cali}$ is the density determined with the Coriolis at the expander's inlet and V_{dis} is the displacement volume.

4.3 Experimental results analysis

A total of 49 points have been recorded. Three of the points have been removed for the realization of the graphs as their values seemed to not follow the trend (probably due to imprecisions in the measurements). As stated in Section 4.1, the main parameters that influence the expander's performance are its rotational speed, the inlet vapor quality, the inlet pressure and the pressure ratio. Those are thus the properties that are varied in the experimental campaigns. The inlet pressure, however, is kept constant during the experiments because it's a property that is very hard to stabilize with this test bench due to the turn on and off of the boiler (see Section 3.4). Two main experimental tests are carried out.

4.3.1 Effect of the inlet vapor quality and of the expander speed

One of the most important objectives of the experimental test campaign is to evaluate the impact of the inlet vapor quality on the performance of the expander. To do so, it was decided to run a series of experiments at different expander speeds while keeping all the other parameters constant except the inlet vapor quality. The inlet pressure is kept constant via the control of the evaporator's hot water temperature and water flow rate. The pressure ratio is fixed by controlling the outlet pressure with the condenser's cold water temperature and water flow rate. The expander speed is tested at different values to have iso-speed performance curves. To vary the inlet vapor quality, the pressure and the temperature at the expander inlet are kept constant while the flow rate is changed via the ORC pump.

In **Figure 4.1**, the evolution of the isentropic and volumetric efficiencies with respect to the vapor quality for four iso-speeds of the expander is plotted. To realize these graphs, the pressure, the temperature at the expander inlet and the pressure ratio are supposed kept constant. In reality, the pressure and the temperature at the expander inlet have some small variations as it is impossible to keep properties constant throughout experiments. As can be observed, decreasing the vapor quality leads to worse performances of the expander in terms of isentropic and volumetric efficiency. In single-phase conditions, the scroll expander has an isentropic efficiency of around 0.6 which is a fair value. However, when the inlet vapor quality decrease, the isentropic efficiency decreases drastically (down to 0.27). This could be explained by the pressure losses that are increasing at the inlet and throughout the discharge port. The expander rotational speed also has a great impact on the isentropic efficiency. As can be seen on **Figure 4.1a**, the isentropic efficiency increases with the speed until 2300 RPM which corresponds to the optimal speed for this pressure ratio. After this speed, the mechanical losses due to the rotational speed increase are too important to get the benefice of the increased work at the shaft. In **Figure 4.1b**, the volumetric efficiency also decreases with decreasing vapor quality. Higher inlet pressure losses and higher leakages could explain this trend. With increasing expander speed, the volumetric efficiency increases as well. This

can be explained by the lower impact of the working fluid leakages through the expander due to the increased expander speed.

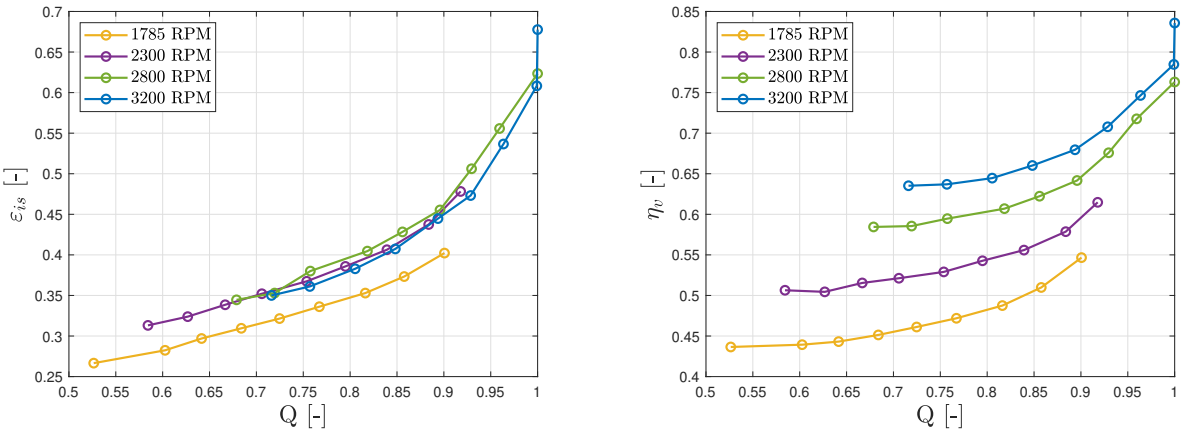

(a) *Evolution of the isentropic efficiency with respect to the inlet vapor quality.*

(b) *Evolution of the volumetric efficiency with respect to the inlet vapor quality.*

Figure 4.1: *Effect of expander inlet vapor quality and speed on the isentropic efficiency and the volumetric efficiency at constant operational parameters (P_{in} = [5.89-5.93] bar, r_p = [2.03-2.1]).*

4.3.2 Effect of the pressure ratio on the expander's performance

The effect of the imposed pressure ratio on the isentropic efficiency under constant rotational speed, inlet pressure and inlet vapor quality are shown in **Figure 4.2**. To vary the pressure ratio, the inlet pressure is kept constant while the outlet pressure is changed via the condenser. In these specific conditions, the maximum isentropic efficiency is at a pressure ratio of about 2.12 which corresponds to the specific volume ratio near the machine built-in volume ratio. The shape of the graph is conform to the literature as the effect of the losses due to the under-expansion and over-expansion are visible.

No variations are visible for the volumetric efficiency in these tests due to the definition which means that the flow going throught the expander is probably chocked.

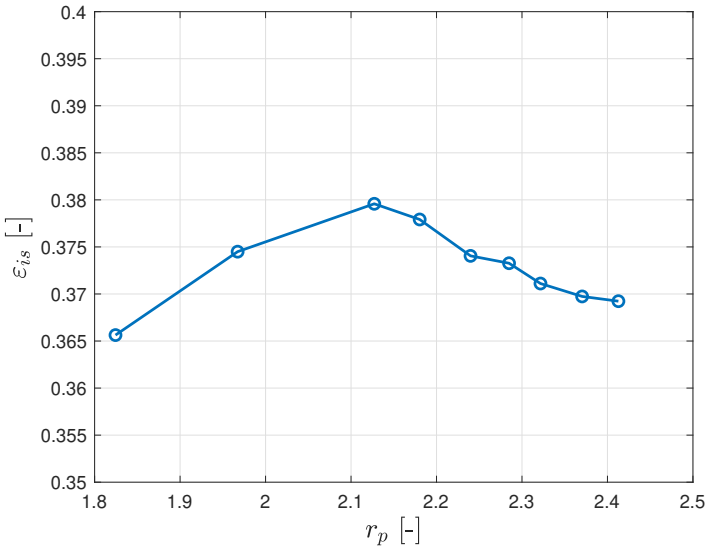

Figure 4.2: *Effect of the pressure ratio on the isentropic efficiency at constant operational parameters (N_{exp} = 1785 RPM, P_{in} = [5.96-6.01] bar, Q = [0.79-0.82]).*

4.4 Data prediction via Gaussian processes

4.4.1 Theoretical background

As well described in Quoilin et al. [38] Gaussian Processes can be useful for the analysis of experimental results.

Gaussian processes (GP) principle

Experimental datasets are always subject to several sources of disturbances, noises, and/or errors, and their impact on the quality of the data should be assessed. The Gaussian method allows us to evaluate the quality of the data and to identify potential outliers.
Gaussian Processes (GP) is a probabilistic model that can be used to perform a regression. The goal of the regression is to find a function that maps each input (the experimental data) to the variable of interest (i.e. isentropic/ volumetric efficiency,...).

First, the unknown function and the hyperparameters are set 'a priori' by the user. That prior is specified in terms of a mean function and a covariance function (also known as a kernel function), which describe the expected mean and covariance of the output values for any given input. By increasing the complexity of the function, the fit of the function to the data can be excellent, however, too complex a model also fits the noise in the data (over-fit).

Once the prior and observed data are specified, the GP regression model uses Bayesian inference to compute the posterior distribution of the unknown function. This posterior can then be used to make predictions of new/unseen data points and provides coherent estimates of predictive uncertainty. Gaussian processes are an interesting tool when working with high-dimensional data and are highly flexible. They are also less subject to over-fitting and the Runge phenomenon and have better behavior outside of the fitting range than traditional linear regression.

Evaluation of the quality of the regression

Once the regression on the experimental data is performed, its quality should be assessed through different numerical indicators. The most common indicator usually calculates the difference between the predicted outputs ($f(x)$) and the true measured values (y). Normalization is necessary as the goal is to compare the model performance across different datasets. Multiples indicators can be used to evaluate the quality of the regression, i.e. the normalized root mean square error (RMSE), the coefficient of determination (R^2), Akaike information criterion (AIC) and the Bayesian information criterion (BIC). For this specific dataset, the Mean Absolute Error (MAE) has been chosen for the evaluation, as this indicator is easy to interpret and is robust to outliers. It is defined with the normalized values (**Equation 4.13**).

$$MAE = \frac{1}{N} \cdot \sum_{i=1}^{N} |y_i' - f(x_i')| \tag{4.13}$$

where $f(x)$ is the GP model prediction for the inputs x.

Cross-validation

The model performance is computed as the ability of the model to predict the target y for new/unseen samples. To evaluate this, the dataset is divided into two: the training set, on which the model is built, and the test set, on which the model performance is evaluated. To split the dataset, the approach used is the cross-validation: the data are partitioned into a fold (e.g., the first 80% of the data are for training and the last 20% are for testing). The dataset is split into many folds in a way that each point ends in the test set once. An example of cross-validation is shown in **Figure 4.3**. A model is made and evaluated through MAE for each fold. The final MAE is computed as the average across all the folds. The cross-validation increases the computational expenses as the analysis has to be repeated for each fold.

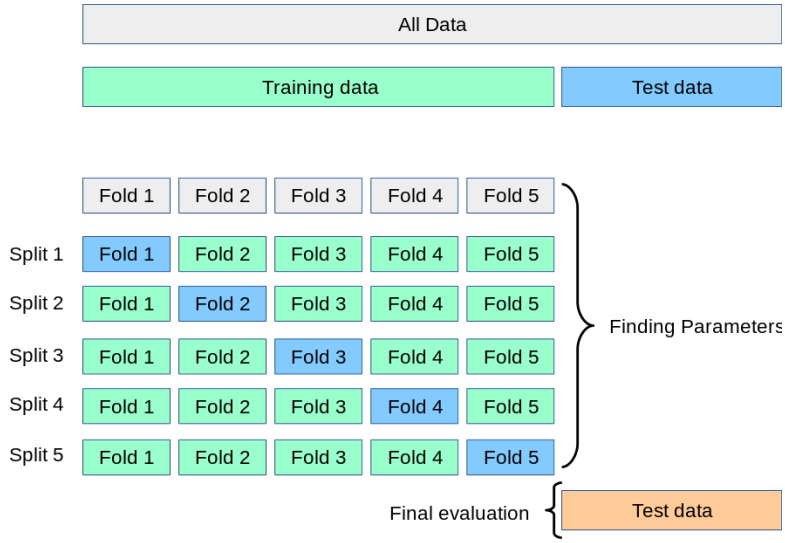

Figure 4.3: *Example of cross-validation. (source : [39])*

An important effect that needs to be detected when performing a regression is ”overfitting”. Overfitting means that the model represents the data too well and captures noise or random fluctuations rather than the underlying patterns or relationships in the data. In case of overfitting, the MAE of the whole dataset should be low (as all of the data should be fitted), while the CV error should be high. To detect risks of overfitting, the ratio between the MAE values of the whole training set (all data points) and the MAE of the CV is evaluated. If this ratio is high there is a risk of overfitting, however, overfitting cannot be quantitatively evaluated and this ratio is just an indicator, this analysis provides a warning, which should be checked visually by plotting the function. A high ratio means that there is a lack of experimental data or too many inputs.

4.4.2 GPExp - A Gaussian Process framework for the analysis of Experimental Data

The implementation of the Gaussian Process for the analysis of Experimental Data is made via the GPExp Open-source library coded in Matlab (Quoilin, S. et al [40]). The inputs of this model are the experimental data gathered in the experimental campaign and the targets are the post-processing results of the expander's performance.

4.4.3 Results analysis

In total, 49 experimental points have been taken. From those points, 3 points have been withdrawn as explained in Section 4.3. Two other points are removed, the points in superheated conditions where the vapor quality is equal to 1. Indeed, those points could have different

degrees of superheating that cannot be taken into account and could impact the isentropic and volumetric efficiency. One last point has been removed as it has been detected as an outlier by GPExp.

In **Figure 4.4**, the dataset versus the prediction and cross-validation for the isentropic and volumetric efficiencies are shown. The distance between the cross-validation point and the test point shows if the model is good or not. As can be seen, the prediction of the volumetric should be better than the prediction of the isentropic efficiency but they are still pretty good.

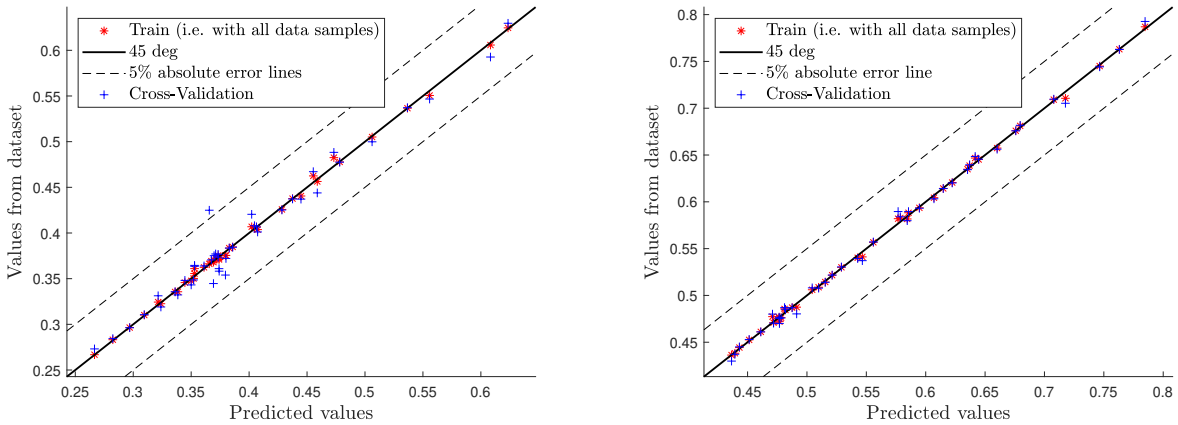

(a) *Dataset versus predictions and cross-validation for the isentropic efficiency.*

(b) *Dataset versus predictions and cross-validation for the volumetric efficiency.*

Figure 4.4: *Dataset versus predictions and cross-validation for different efficiencies.*

In **Table 4.3**, the MAE of the prediction and the CV are shown, as well as their ratio. For the isentropic efficiency, the ratio between the error in CV and training is 3.66. This value is between 2 and 4, which might indicate some overfitting. This needs to be validated visually. This problem is probably caused by a lack of experimental data. However, the volumetric efficiency seems to be well predicted.

Table 4.3: *Mean absolute values of the prediction (MAE_{pred}) and of the cross-validation (MAE_{CV}) and their ratio.*

	MAE_{pred}	MAE_{CV}	$\frac{MAE_{CV}}{MAE_{pred}}$
ε_{is}	0.62105 %	2.3223 %	3.74
ε_{v}	0.59812 %	1.0328 %	1.73

A graphical representation of where the points have been recorded is shown in **Figure 4.5**.

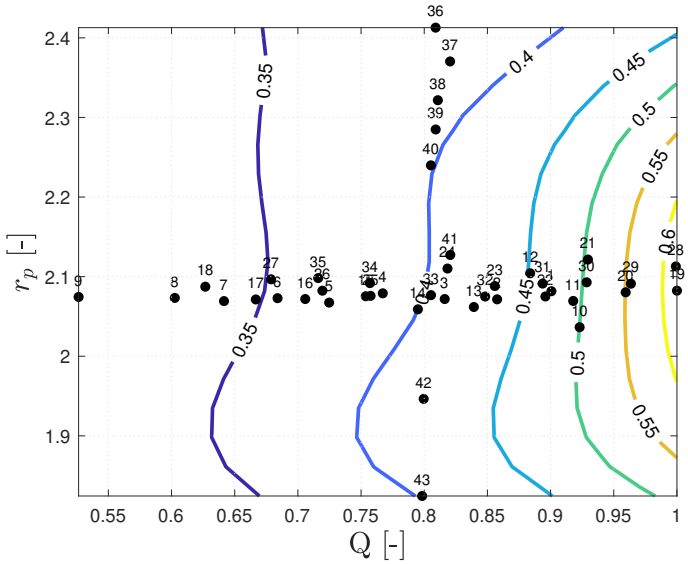

Figure 4.5: *Representation of the recorded points on a 2D map with the isolines of the isentropic efficiency (inlet quality and pressure ratio) with an inlet pressure of 6 bar, ans an expander speed of 2500 RPM.*

Isentropic efficiency

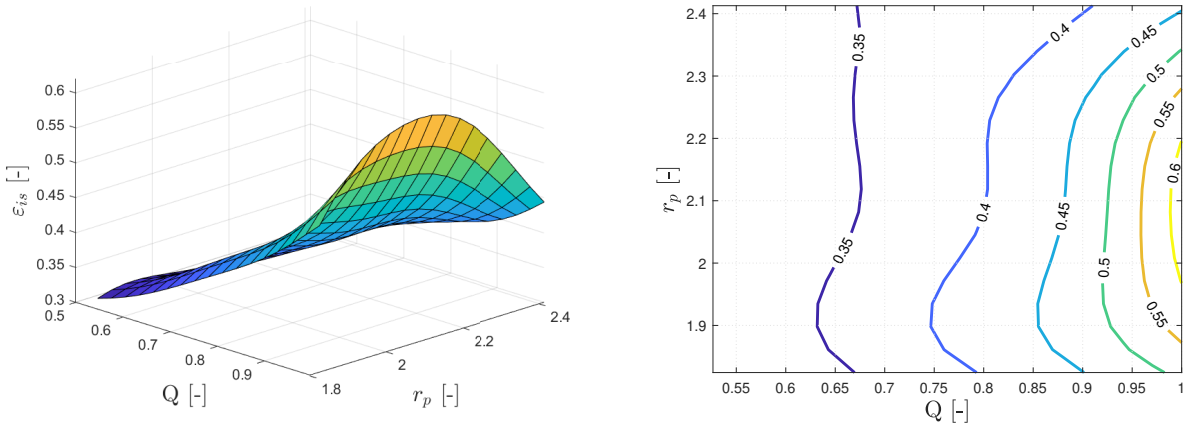

(a) *3D map.*

(b) *Isoline of the isentropic efficiency map.*

Figure 4.6: *Evolution of the isentropic efficiency with respect to the inlet quality and the pressure ratio for an inlet pressure of 6 bar and an expander speed of 2500 RPM.*

The variables influencing the isentropic efficiency are the inlet vapor quality, the expander's speed, the pressure ratio and the inlet pressure. Another variable that could potentially influence the isentropic efficiency is the OCR, unfortunately, only one OCR has been tested and

studying its impact is thus not possible in this thesis. In the same way, the narrow range tested of the inlet pressure does not allow for studying its impact. In **Figure 4.6**, the isentropic efficiency is plotted with respect to the vapor quality and the pressure ratio as they are the variables with the biggest influence. The inlet pressure and the expander speed are fixed. As predicted, some overfitting is visually recognizable.

As already explained in Section 4.3.1, the isentropic efficiency decreases with the inlet vapor quality. In **Figure 4.6b**, the lowest isentropic efficiency is found for the lowest vapor quality (around 0.5) and the highest pressure ratio (around 2.4).

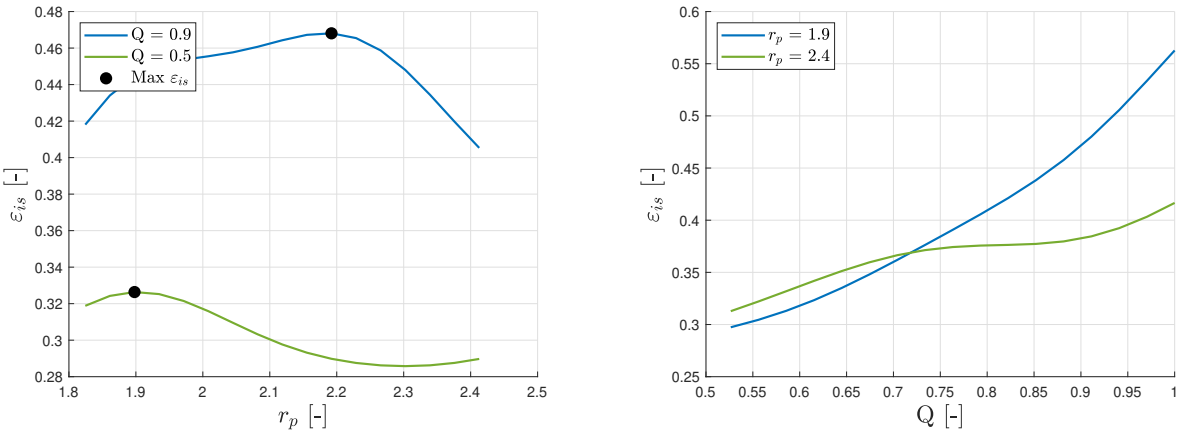

(a) *Isentropic efficiency versus pressure ratio for two vapor qualities.*

(b) *Isentropic efficiency versus vapor qualities for two pressure ratio.*

Figure 4.7: *2D evolution of the isentropic efficiency for an inlet pressure of 6 bar and an expander speed of 2500 RPM.*

In **Figure 4.7a**, the isentropic efficiency is plotted with respect to the pressure ratio for two different vapor qualities. One can see that the optimal pressure ratio (the one for which the isentropic efficiency is maximal) is not the same for both vapor qualities. Indeed, the optimal pressure ratio seems ”shifted” towards a lower pressure ratio for the lowest vapor quality. This effect could be explained by the outlet-inlet volume ratio that is closer to the built-in volume ratio when lowering the pressure ratio for lower vapor quality. In **Figure 4.7b**, the isentropic efficiency is plotted with respect to the vapor quality for two different pressure ratios. There seems to be an optimal vapor quality corresponding to each pressure ratio. Under-expansion losses appear to be emphasized with low vapor qualities.

Influence of the speed

In **Figure 4.8**, the iso-efficiency cartography is plotted for two different speeds. For high vapour qualities, increasing the expander speed improves the isentropic efficiency while for

low vapour qualities, it seems to deteriorate them. Indeed, one possible explanation is that higher vapour qualities expansions are more prone to leakage losses and increasing the speed reduces the leakages, while lower vapour qualities expansions are more prone to pressure drops which are increased when increasing the speed.

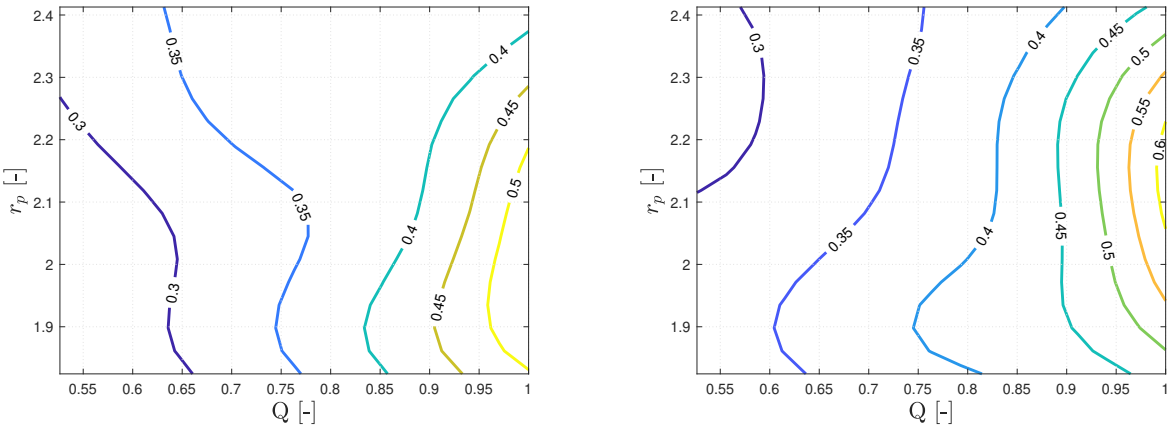

(a) *Isoline of the isentropic efficiency map at 1800 RPM.*

(b) *Isoline of the isentropic efficiency map at 3100 RPM.*

Figure 4.8: *Evolution of the isentropic efficiency with respect to the inlet quality and the pressure ratio for an inlet pressure of 6 bar.*

Power at the shaft

The work at the shaft is also mainly affected by the pressure ratio, the speed and the inlet vapor quality. In **Figure 4.9**, the power at the shaft with respect to the vapor quality and the pressure ratio is plotted. In general, the power seems to increase with the pressure ratio and the vapor quality. Indeed, more pressure work is converted into mechanical work at a greater pressure ratio and lowering the vapour quality means increasing the viscosity of the fluid which decreases the power produced by the expander. The power seems to decrease after a certain pressure ratio. This observation is surprising as the power should increase continuously with the pressure ratio.
In **Figure 4.10**, the power is plotted with respect to the pressure ratio and the expander speed as this second variable greatly impacts the work at the shaft. It is plotted for two values of the inlet vapor quality. As can be seen, the power increases with the speed and the pressure ratio, which is expected.

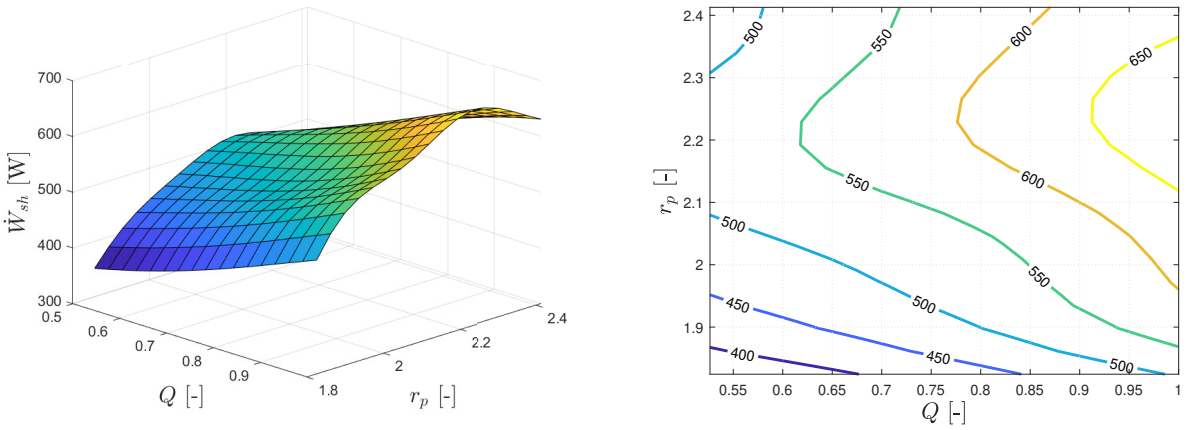

(a) *3D map.* **(b)** *Isoline of the power at the shaft map.*

Figure 4.9: *Evolution of the power at the shaft with respect to the inlet vapor quality and the pressure ratio for an inlet pressure of 6 bar and an expander speed of 2500 RPM.*

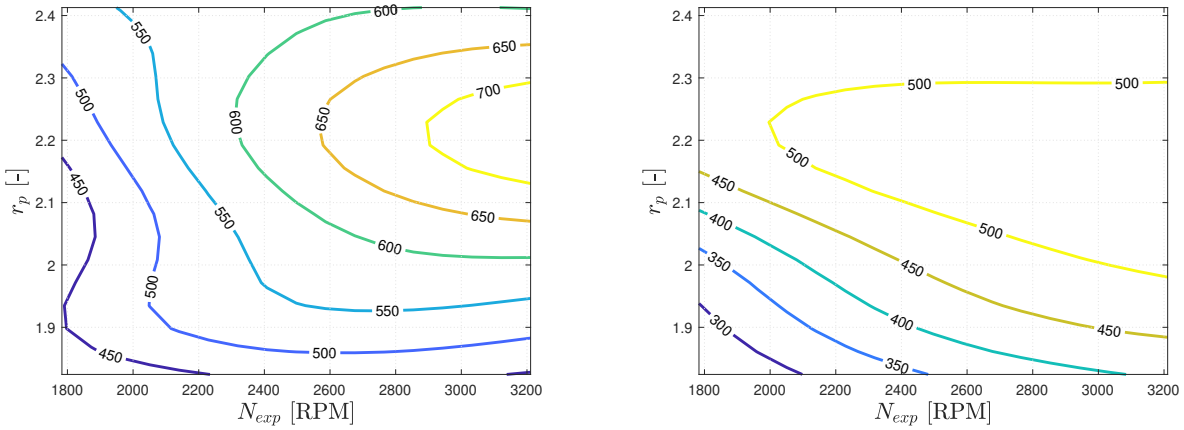

(a) *Isoline of the power at the shaft map. (Q=0.9)* **(b)** *Isoline of the power at the shaft map. (Q=0.5)*

Figure 4.10: *Evolution of the isentropic efficiency with respect to the inlet quality and the pressure ratio for an inlet pressure of 6 bar.*

Volumetric efficiency

Once again, the most influential variables on the volumetric efficiency are the pressure ratio, the inlet quality and the speed. In **Figure 4.11**, the volumetric efficiency is plotted versus the vapor quality and the pressure ratio. As stated in Section 4.3.1, the volumetric efficiency decreases with the inlet quality. The higher inlet pressure losses and the leakage could explain this shape. At lower vapor quality, the volumetric efficiency decreases with increasing pressure ratio. However, after a certain vapor quality (around 0.8), the pressure ratio has almost no impact on the volumetric efficiency. This could be explained by a choked flow at higher vapor quality.

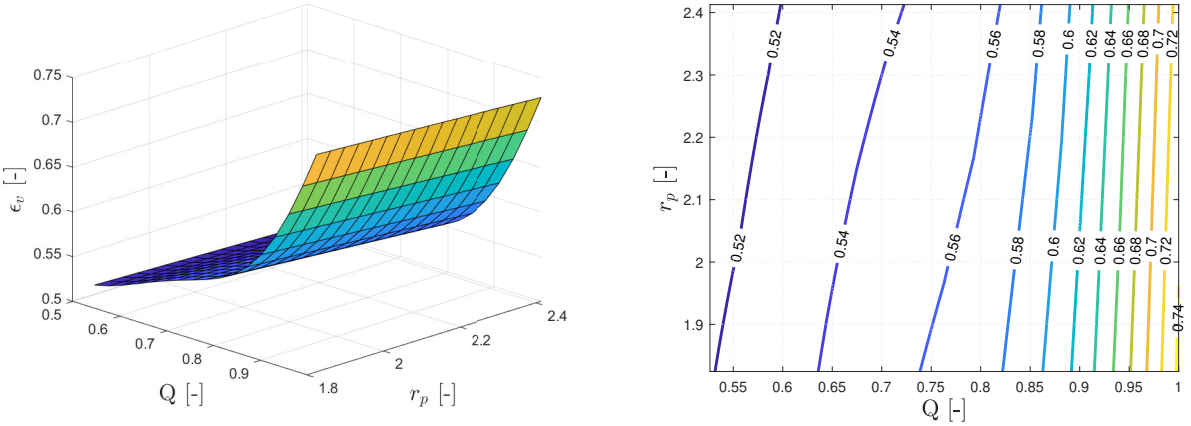

(a) *3D map.* **(b)** *Isoline of the volumetric efficiency map.*

Figure 4.11: *Evolution of the volumetric efficiency with respect to the inlet quality and the pressure ratio for an inlet pressure of 6 bar and a compressor speed of 2500 RPM.*

Influence of the speed

The influence of the speed can be observed in **Figure 4.12**. Increasing the speeds has a positive impact on the volumetric efficiency as it decreases the leakages. The impact is greater for higher qualities as the losses due to leakages have a greater impact on higher qualities.

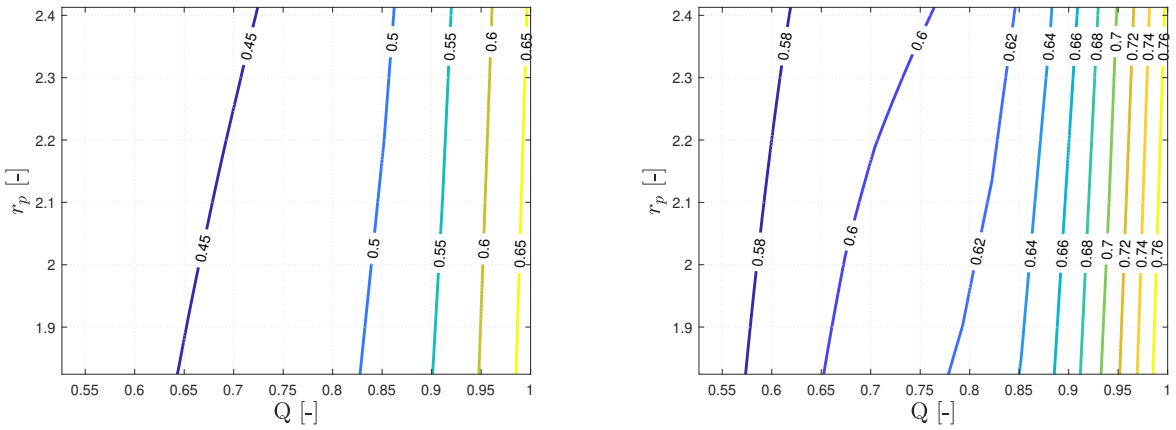

(a) *Isoline of the volumetric efficiency map (1800 RPM).*

(b) *Isoline of the volumetric efficiency map (3100 RPM).*

Figure 4.12: *Evolution of the volumetric efficiency with respect to the inlet quality and the pressure ratio for an inlet pressure of 6 bar.*

Mass flow rate

The same variables influence the mass flow rate. In **Figure 4.13**, the mass flow rate is plotted versus the expander speed and the pressure ratio. The mass flow rate increases with increasing expander speed and decreasing pressure ratio. Indeed, leakages are decreased with increasing expander speed but are increased with increasing pressure ratio.

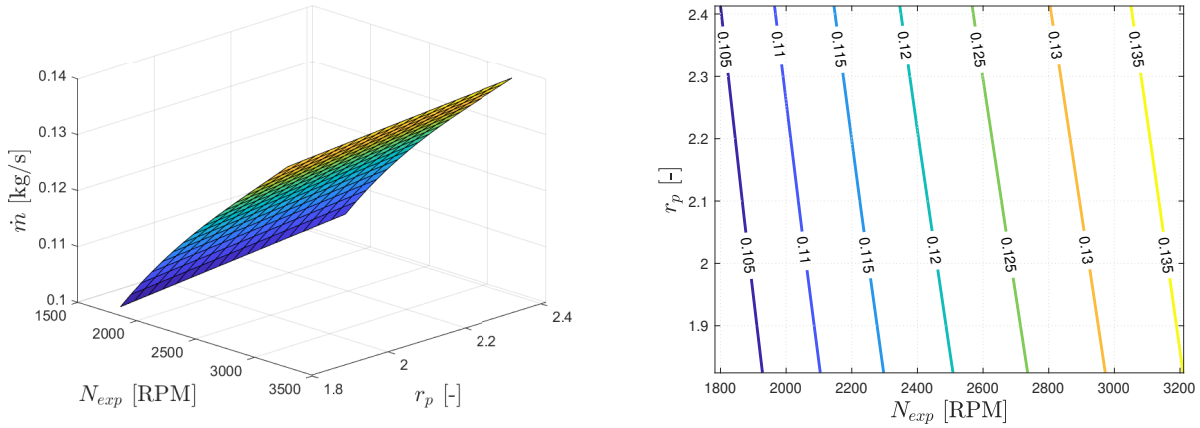

(a) *3D map.*

(b) *Isoline of the mass flow rate map.*

Figure 4.13: *Evolution of the mass flow rate with respect to the expander speed and the pressure ratio for an inlet pressure of 6 bar and a vapor quality of 0.8.*

Chapter 5

Semi-empirical model of the expander

5.1 Modelling of the scroll expander in two-phase

5.1.1 Assumptions

Several assumptions are necessary to evoke:

- The first noticeable assumption made is that the oil has a negligible impact on the model. In fact, a model taking into account the oil is proposed in Section 5.2, unfortunately, its validation was not successful.
- As stated previously, thermodynamics equilibrium is assumed before the expander and the temperature of the mixture is supposed to be the same for the vapor and liquid phases.
- The specific heats at constant pressure (c_p) values are supposed to be equal to their values in one phase. Indeed, their values in the two-phase region could tend towards infinity.

5.1.2 Semi-empirical model

The semi-empirical model of the expander is based on the model proposed by (V. Lemort et al., 2009 [41]).

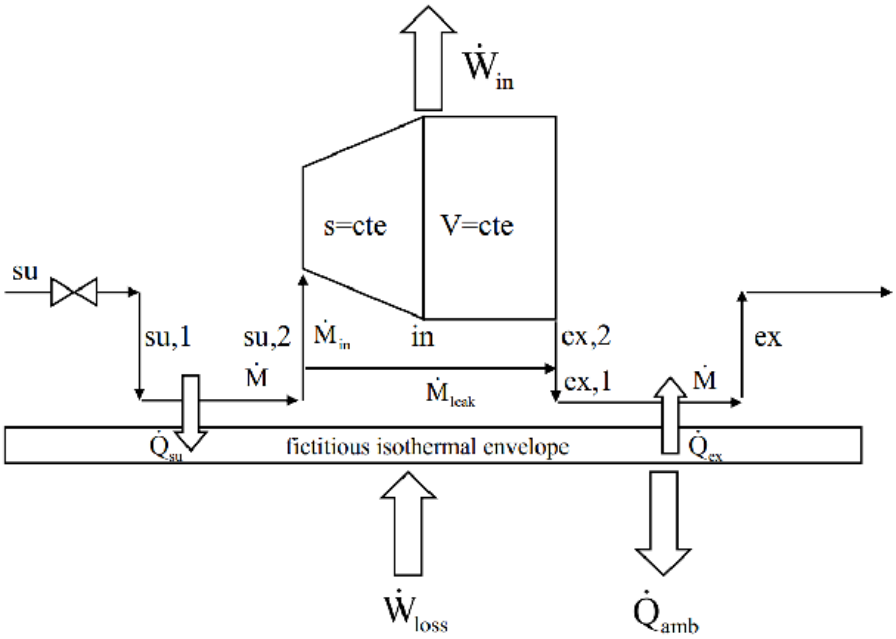

Figure 5.1: *Scheme of the expander model. (source :[41]*

The evolution of the refrigerant through the expander is decomposed into 6 thermodynamical processes:

- su $\rightarrow$ su1: Supply pressure drop
- su1 $\rightarrow$ su2: Cooling at the entrance
- su2 $\rightarrow$ in: Isentropic expansion to internal pressure imposed by the built-in ratio
- in $\rightarrow$ ex2: Isochoric expansion
- ex2 $\rightarrow$ ex1: Adiabatic mixing between supply and leakage flows
- ex1 $\rightarrow$ ex: Heating at the exit

Supply pressure drop

The supply pressure drop ($\Delta P_{su} = P_{su,1} - P_{su}$) takes into account the pressure losses from the suction line to the suction chamber of the expander. The real flow of the fluid is modelled by a flow in a nozzle simply convergent followed by a diffuser. In the nozzle, the flow is supposed isentropic while in the diffuser, the flow is supposed completely irreversible (the kinetic energy of the fluid is lost and not converted into static pressure). The whole process is supposed to be isenthalpic if the kinetic energy between the entrance and the exit is negligible.

The modelization is composed of two stages; an isentropic expansion until the throat and even after the throat if the critical pressure ratio is exceeded and then an isobaric evolution where the kinetic energy is converted into static enthalpy, which represents the pressure loss.

The process is modelled by the following equations:

$$P_{thr,su} = max(P_{su,1}, P_{crit,su}) = max(P_{su,1}, P_{su} \cdot \frac{2}{\gamma_{su}+1}^{\frac{\gamma_{su}}{\gamma_{su}-1}}) \tag{5.1}$$

Where $\gamma_{su} = \frac{C_{p,su}}{C_{v,su}}$. If the flow is choked, the pressure at the throat is equal to the pressure at the outlet of the diffusor ($P_{su,1}$). The enthalpy is then determined via **Equation 5.2**.

$$h_{su,1} = h_{su} = h_{thr,su} + \frac{C_{su}^2}{2} \tag{5.2}$$

Where $C_{su} = \frac{\dot{m} \cdot v_{thr,su}}{A_{su,1}}$ is the flow speed and the end of the diffuser and $A_{su,1} = \pi \cdot \frac{d_{su,1}^2}{2}$. $d_{su,1}$ is the diameter and the parameters to calibrate to represent the supply pressure drop.

Heat transfers

Different heat transfers take place at the entrance and exhaust of the expander:

- Between the expander shell and the fluid at the entrance and exhaust in the pipes.
- Between the scrolls of the expander and the fluid present in the suction and discharge chambers.
- Between the shell and the ambient.

Those heat transfers are evaluated by introducing a fictitious isothermal envelope at the wall temperature T_w. The internal face of the envelope is in contact with the fluid in the expander and the external face is in contact with the ambient.

$$\epsilon_{su/ex} = 1 - e^{-\frac{Au_{su/ex}}{C_{vsu/ex}}} \tag{5.3}$$

$$\dot{Q}_{su/ex} = \epsilon_{su/ex} \cdot \dot{C}_{su/ex} \cdot (T_w - T_{su,1/ex,1}) \tag{5.4}$$

$$AU_{su/ex} = AU_{su,n/ex,n} \cdot \frac{\dot{m}}{\dot{m}_n}^{0.8} \tag{5.5}$$

Two new parameters are introduced; the heat transfer coefficients $AU_{su,n/ex,n}$.

Leakages

The presence of leakages in expanders can greatly impact the volumetric efficiency of expanders, especially without oil. Leakages in a scroll expander can come from two different phenomena [42]:

- A radial leakage due to the gap between the bottom or the top plate
- A flank leakage resulting from a gap between the flanks of the scrolls

The leakages are modeled in the same way as the pressure drop. Unlike the pressure losses at the suction, it is not rare to have a choked flow for the leakages. Indeed, the critical pressure could be greater than the exhaust pressure as this one is smaller than the supply pressure.

$$P_{thr,leak} = max(P_{ex,2}, P_{crit,leak}) = max(P_{ex,2}, P_{su,2} \cdot \frac{2}{\gamma_{leak}+1}^{\frac{\gamma_{leak}}{\gamma_{leak}-1}}) \tag{5.6}$$

$$h_{su,2} = h_{thr,leak} + \frac{C_{thr,leak}^2}{2} \tag{5.7}$$

Where $C_{thr,leak}$ is the speed of the flow at the throat. The leakage mass flow rate can be determined from the mass conservation equation (**Equation 5.8**).

$$\dot{m}_{leak} = \frac{A_{leak}}{v_{thr,leak}} \cdot C_{neck,leak} \tag{5.8}$$

The mixing between the leakage flow and the flow entering the scroll expander is supposed to be adiabatic and the state after mixing is determined with **Equation 5.9**.

$$h_{ex,1} \cdot \dot{m} = h_{ex,2} \cdot \dot{m}_{in} + h_{su,2} \cdot \dot{m}_{leak} \tag{5.9}$$

This loss introduces a new parameter to calibrate A_{leak}, the throat area.

Expansion

The expansion inside the scroll expander is modeled in two stages; first as an isentropic expansion up to the internal pressure (P_{in}) and then by an isochoric expansion up to the exhaust pressure (P_{ex}). The internal pressure P_{in} is evaluated via the entropy ($s_{su,2} = s_{in}$) and the specific volume v_{in} that is evaluated with respect to the built-in ratio:

$$v_{in} = v_{su,2} \cdot r_{v,in} \tag{5.10}$$

If the pressure P_{in} is different than the exhaust pressure P_{ex}, then the expansion is not adapted to the built-in ratio and the fluid is either over-expanded (if $P_{ex} > P_{in}$) or under-expanded (if $P_{ex} < P_{in}$).
The internal work made by the expander is calculated via **Equation 5.11**.

$$\dot{W}_{in} = \dot{m}_{in} \cdot (w_s + w_v) \tag{5.11}$$

Where w_s is the work made during the isentropic process and w_v is the work made during the isochoric process.

Energy balance over the expander

The energy balance over the expander is the following:

$$\dot{W}_{loss} + \dot{Q}su - \dot{Q}_{ex} - \dot{Q}_{amb} = 0 \tag{5.12}$$

Where $\dot{W}_{loss}$ accounts for the mechanical losses (**Equation 5.13**).

$$\dot{W}_{loss} = 2\pi \cdot \frac{N_{exp}}{60} \cdot T_{loss} \tag{5.13}$$

The parameter used to model this loss is the torque loss, T_{loss},
$\dot{Q}_{amb}$ accounts for the losses made to the ambient (**Equation 5.14**).

$$\dot{Q}_{amb} = AU_{amb} \cdot (T_w - T_{amb}) \tag{5.14}$$

Wich introduces the heat transfer coefficent AU_{amb} as a new parameter.

5.1.3 Information diagram of the expander model

The information diagram of the model is shown in **Figure 5.2**. The input variables of the model are the supply pressure, the pressure ratio, the supply vapor quality and the expander speed. The outputs of the model are the mass flow rate and the power produced at the shaft. The model necessitates 8 parameters.

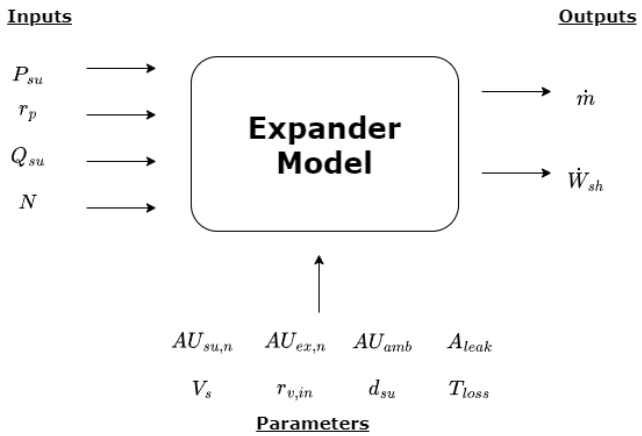

Figure 5.2: *Information diagram of the expander semi-empirical model.*

5.1.4 Model calibration with the experimental datas

After developing the model, it needs to be fitted to the experimental data. To calibrate the model, two variables are checked; the power at the shaft ($\dot{W}_{sh}$) and the mass flow rate ($\dot{m}$). The mass flow rate checked is the mass flow rate of the refrigerant only as the oil has not

been taken into account in this model. The calibration was made by checking on the graphs, available in **Figure 5.3**, different sets of parameters to find the one where the data points were the closest to the 45° line. The error global error function ϵ needs to be minimized (**Equation 5.15**).

$$\epsilon = \frac{1}{2}\sqrt{\sum_{1}^{N_{\text{tests}}}\left(\frac{\dot{m}_{\text{calc}} - \dot{m}_{\text{meas}}}{\dot{m}_{\text{calc}}}\right)^2} + \frac{1}{2}\sqrt{\sum_{1}^{N_{\text{tests}}}\left(\frac{\dot{W}_{\text{sh, calc}} - \dot{W}_{\text{sh, meas}}}{\dot{W}_{\text{sh, calc}}}\right)^2} \tag{5.15}$$

As can be observed in **Figure 5.3a**, the calibration of the mass flow rate is not ideal. In fact, when trying to calibrate the model with the vapor quality determined based on the Coriolis (see Section 3.3.7), the slope of the data points was never able to meet the 45° line. In fact, after checking the experimental data, there was a mismatch in the heat balance between the waterside and the refrigerant side of the evaporator. Yet, the density measured by the Coriolis is calibrated based on that heat balance. The quality has then been recalculated with the heat balance on the evaporator, by taking into account a loss of 13% between the water and the refrigerant side. The calculation of the mass flow rate with the model was better with the newly calculated vapor quality. The results analyzed are thus not entirely representative of the experimental results. The average error (MAE) between the predictions and the measurement is 0.011 kg/s for the mass flow rate which is a rather bad value considering the average mass flow rate of the measurements is 0.1 kg/s (represents 11% of errors on the average). The prediction of the mass flow rate seems to be underrated. The MAE of the power at the shaft is 30 W for a mean value of the measurements of 534 W (represents 5.6 % of errors on the average).

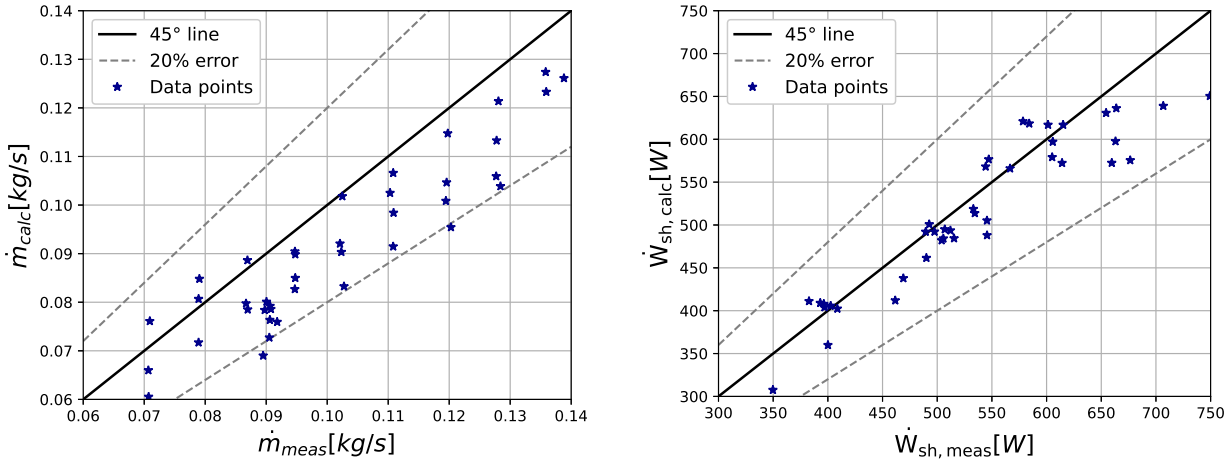

(a) *Shaft power prediction of the expander model versus experimental data (MAE = 0.011 kg/s).*

(b) *Mass flow rate prediction of the expander model versus experimental data (MAE = 30 W).*

Figure 5.3: *Prediction versus experimental data.*

The parameters that are determined are available in **Table 5.1**.

Table 5.1: *Model parameters.*

Parameter	Value
V_s	86 cm^3
$r_{v,in}$	2
$d_{su,1}$	8.7 mm
$AU_{su,n}$	20 W/K
A_{leak}	6.5 mm^2
$AU_{ex,n}$	30 W/K
T_{loss}	0.7 N-m
AU_{amb}	5 W/K

5.1.5 Results analysis

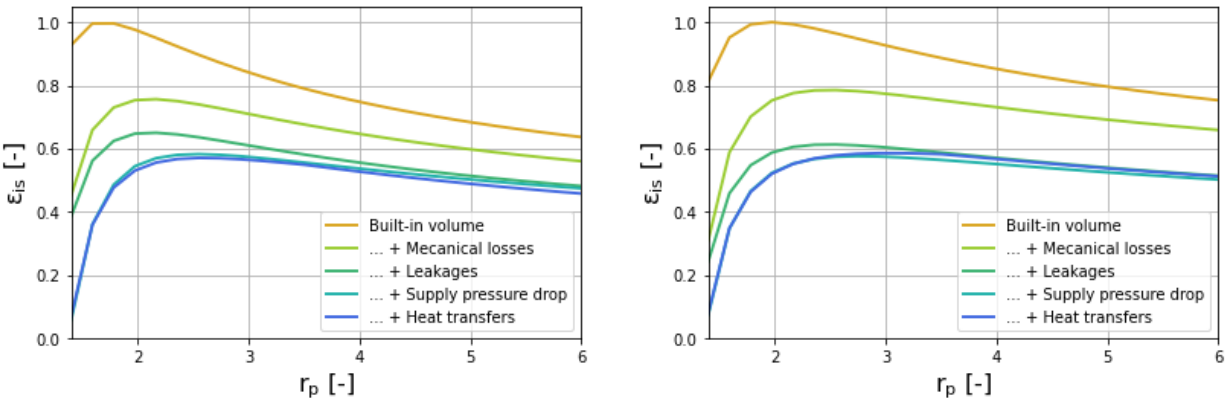

(a) *Q = 0.4* **(b)** *Q = 0.9*

Figure 5.4: *Isentropic efficiency versus the pressure ratio with the losses contribution in the expander model (P_{su} = 6 bar, N_{exp} = 2500 RPM).*

In **Figure 5.4**, the isentropic efficiency with respect to the pressure ratio with the different sources of losses is plotted for two vapor qualities. In both cases, the mechanical losses have a great impact on the degradation of the isentropic efficiency. This could be explained by the increase of the viscosity of the fluid. The leakages also greatly contribute to the diminution of the isentropic efficiency. However, the impact is greater for the flow with less liquid (Q = 0.9). Indeed, the liquid acts as a ”sealant” and less leakage appears in a two-phase flow. The losses due to the supply pressure drop have more impact on the expansion with 0.4 vapor

quality. Indeed, the denser the fluid the bigger the pressure losses. The losses due to the heat transfer are minimal.
In **Figure 5.5**, the isentropic efficiency with respect to the expander speed with the different sources of losses is also plotted for two vapor qualities. Once again, one can see that the leakage losses seem to have more impact on the graph with the highest vapor quality (Q=0.9) while the pressure losses seem to have more impact on the graph with the lowest vapor quality (Q=0.4).

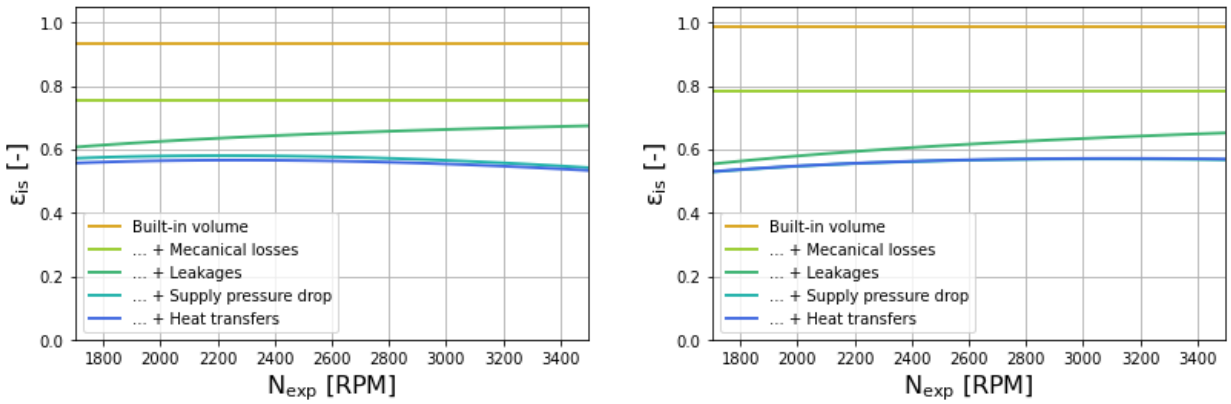

(a) *Q = 0.4.* **(b)** *Q = 0.9.*

Figure 5.5: *Isentropic efficiency versus the expander speed with the losses contribution in the expander model (P_{su} = 6 bar, r_p = 2.3).*

In **Figure 5.6**, the isentropic efficiency versus the pressure ratio for two vapor qualities and two different expander speeds is plotted. The first observation is that the optimal pressure ratio seems to be shifted depending on the vapor quality. This has been observed also experimentally and can be explained by the fact that the outlet-inlet volume ratio that is closer to the built-in ratio when decreasing the pressure ratio for lower vapor quality. Another observation is that the optimal pressure ratio is also shifted with the expander speed. The losses due to the speed increase are more present for the lower vapor quality. Indeed, at lower speeds, leakages have more impact than at higher speeds but, as stated previously, there is less leakage at lower vapor quality. However, at higher speeds, there are more friction losses and more pressure drops for which the two-phase flows are more impacted. It also seems that there are fewer losses in the under-expansion region for the higher vapor quality (Q = 0.9). Increasing the built-in ratio would yield better performance for the higher pressure ratio for the lower quality.

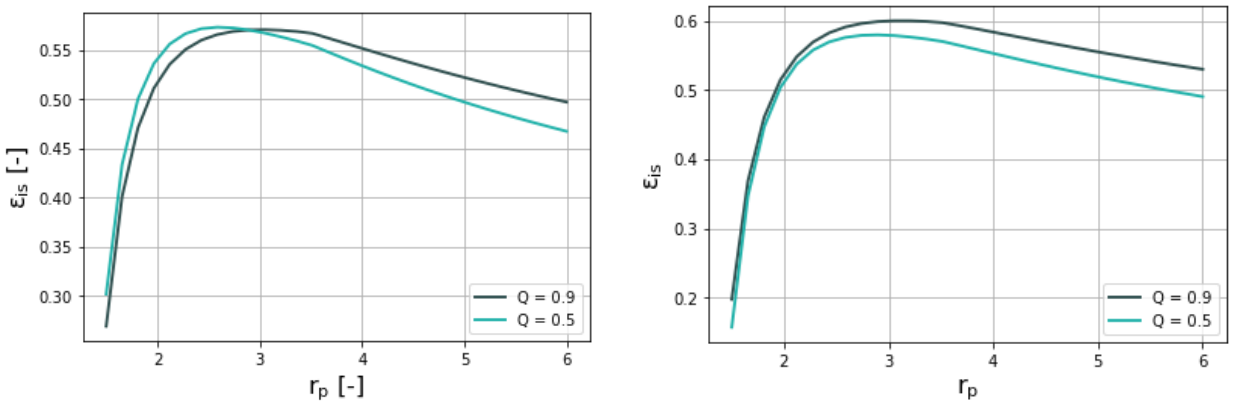

(a) N_{exp} = *2100 RPM.* **(b)** N_{exp} = *3200 RPM.*

Figure 5.6: *Isentropic efficiency versus the pressure ratio for two different vapor qualities (P_{su} = 6 bar).*

Depending on the inlet vapor quality of the expander, the expander speed can have more or less impact on the isentropic efficiency as is depicted in **Figure 5.7** and already observed. Under-expansion losses have more impact on the lower vapor quality as already discussed previously. For the pressure ratio equal to 2, it seems that at around 2900 RPM, the isentropic efficiency is the same for both vapor qualities. For the pressure ratio equal to 4 that isentropic efficiency equilibrium seems to be at lower speeds than 1800 RPM.

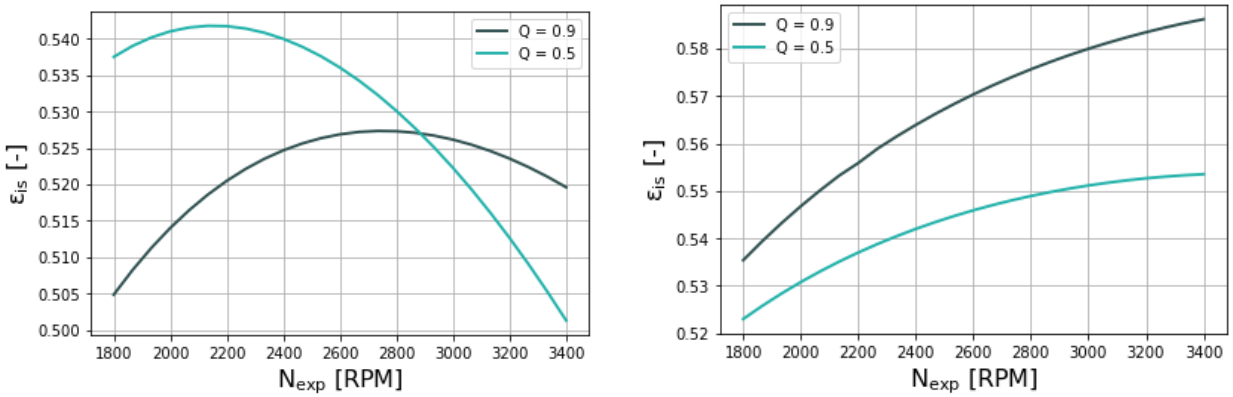

(a) r_p = *2.* **(b)** r_p = *4.*

Figure 5.7: *Isentropic efficiency versus the expander speed for two different vapor qualities (P_{su} = 6 bar).*

In **Figure 5.8**, the volumetric efficiency is plotted with respect to the expander speed for two different inlet qualities and two different pressure ratios. As usual, the volumetric efficiency

is always better when increasing the expander speed. The volumetric efficiency is better when the vapor quality is equal to 0.5 than to 0.9, which is the opposite of the experimental results. This could be explained by an overestimation of the leakage losses. When increasing the pressure ratio, the volumetric efficiencies seem to increase only for the curve with the vapor quality equal to 0.9. Indeed, for the lower vapor quality, the flow seems to be chocked.

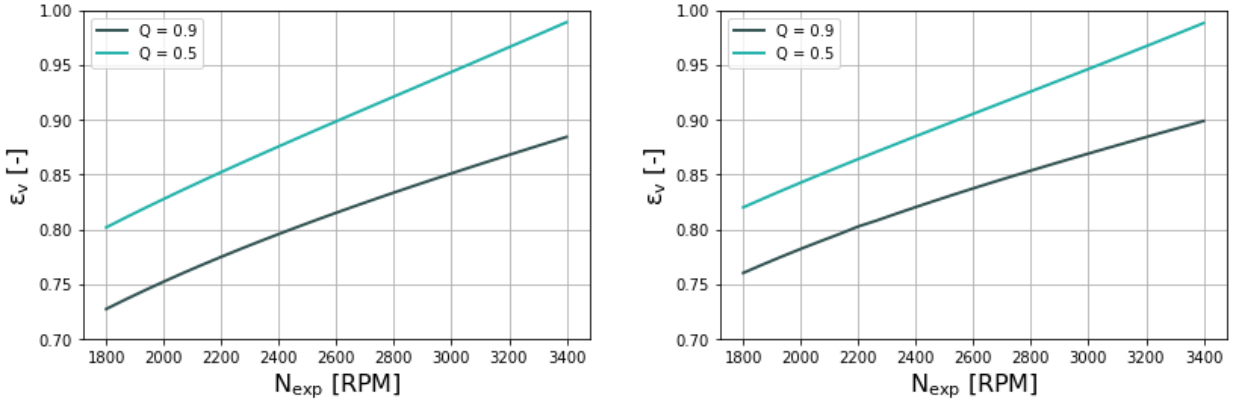

(a) $r_p = 2$. **(b)** $r_p = 4$.

Figure 5.8: *Volumetric efficiency versus the expander speed for two different vapor qualities (P_{su} = 6 bar).*

Two effects are to take into account when calculating the volumetric efficiency; the leakages and the effect of the supply pressure drop and the heat transfers. Following this decomposition, the volumetric efficiency definition can also be decomposed [43].

$$\varepsilon_v = \frac{\dot{m_{th}}}{\dot{m}} = \frac{\dot{m_{in}}}{\dot{m}} \cdot \frac{\dot{m_{th}}}{\dot{m_{in}}} = \varepsilon_{v,l} \cdot \varepsilon_{v,PT} \tag{5.16}$$

The theoretical mass flow rate is defined according to the expander's speed, the swept volume V_s and the conditions at the expander inlet;

$$\dot{m_{th}} = iN \cdot \frac{V_s}{v_{su}} \tag{5.17}$$

i is the working cycle frequency and is defined as the number of pressure-volume diagrams described by the fluid per rotation of the expander shaft (equal to one in this case).
In **Figure 5.9**, the different definitions of the volumetric efficiency are plotted with respect to the expander speed for two vapor qualities. Both effects impact the volumetric efficiency. $\varepsilon_{v,PT}$ represents the effect of the pressure drop and the heat transfer on the volumetric efficiency. It increases with the expander speed as the heat transfers and pressure drops decrease with increasing speed which decreases $\dot{m}_{in}$. $\varepsilon_{v,l}$ represents the impact of the leakages on the volumetric efficiency, and as expected, they decrease with increasing speed.

As previously stated, volumetric efficiency is better for the lowest vapor quality. $\varepsilon_{v,PT}$ seems to variate more when the vapor quality is equal to 0.5 as the specific volume changes more.

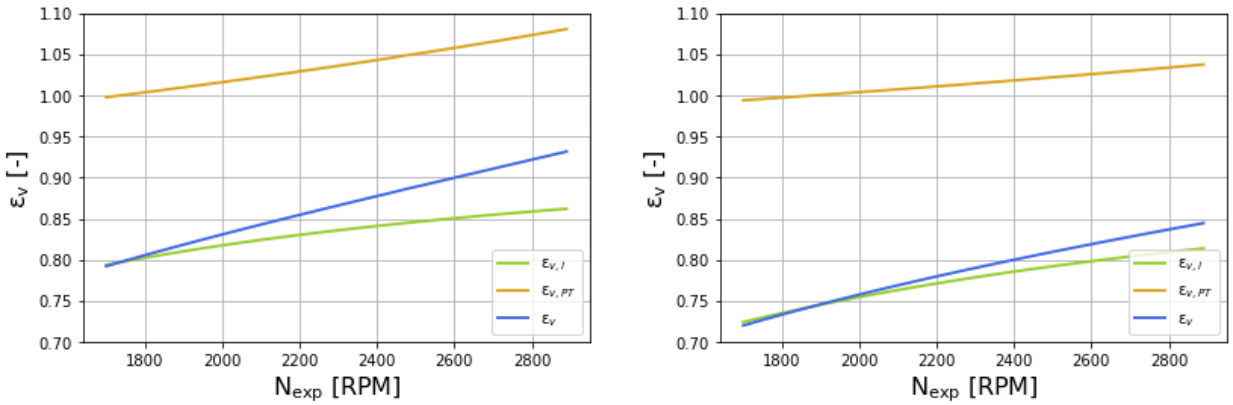

(a) *Q = 0.5.* **(b)** *Q = 0.9.*

Figure 5.9: *Different definitions of the volumetric efficiency versus the expander speed for two different vapor qualities ($P_{su} = 6$ bar, r_p = 2.3).*

The isentropic efficiency can also be decomposed into its different impact (**Equation 5.18**). η_m is the mechanical efficiency of the expander and $\varepsilon_{is,th}$ is the theoretical isentropic effectiveness.

$$\varepsilon_{is} = \frac{\dot{W}_{sh}}{\dot{W}_s} = \frac{\dot{W}_{sh}}{\dot{W}_{in}} \cdot \frac{\dot{W}_{in}}{\dot{m}_{th} \cdot w_s} \cdot \frac{\dot{m}_{th}}{\dot{m}} = \eta_m \cdot \varepsilon_{is,th} \cdot \varepsilon_v \tag{5.18}$$

In **Figure 5.10**, the different contributions to the isentropic efficiency are plotted with respect to the expander speed for two vapor qualities. As already stated, the volumetric efficiency is better for the lower vapor quality while the theoretical isentropic effectiveness is worse than the higher vapor quality. The mechanical efficiency stays the same for both graphs as its value only changes with the rotational speed.
In **Figure 5.11**, the different contributions of the isentropic efficiency are plotted versus the pressure ratio.

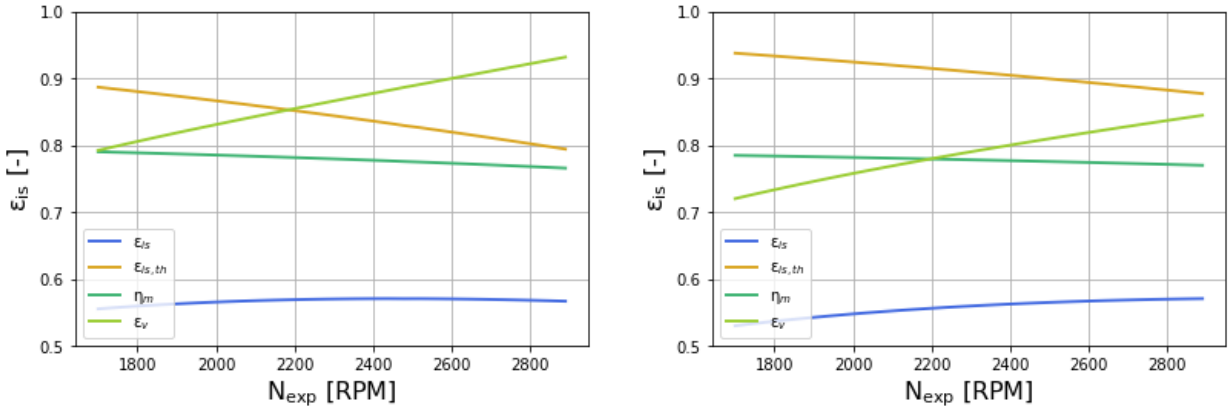

(a) $Q = 0.5$. **(b)** $Q = 0.9$.

Figure 5.10: *Different definitions of the isentropic efficiency versus the expander speed for two different vapor qualities ($P_{su} = 6bar$, r_p = 2.3).*

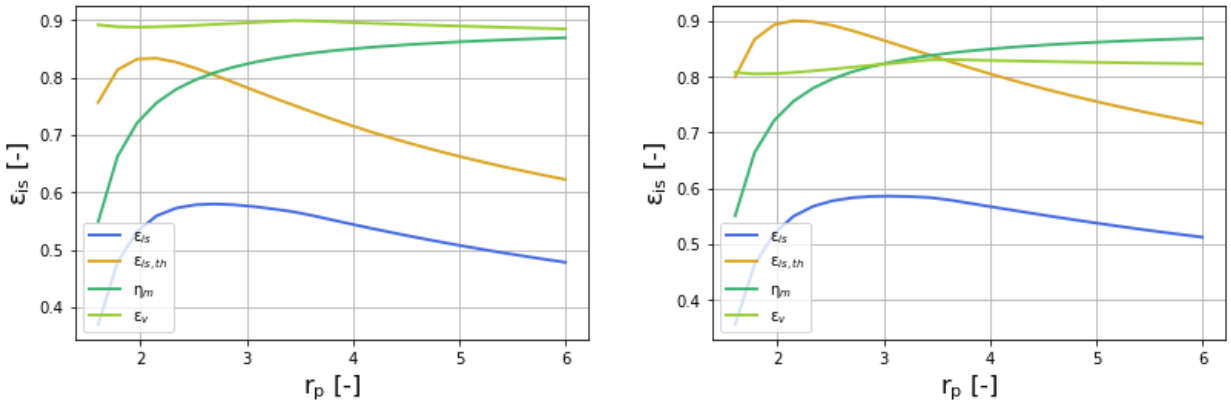

(a) $Q = 0.5$. **(b)** $Q = 0.9$.

Figure 5.11: *Different definitions of the isentropic efficiency versus the pressure ratio for two different vapor qualities ($P_{su} = 6$ bar, N_{exp} = 2500 RPM).*

5.1.6 Investigation for two-phase amelioration

Some of the losses encountered when working with a two-phase flow are due to under expansion losses that are accentuated. One way to solve this problem would be to change the geometry of the scroll expander. To do so, two geometrical parameters are available; the swept volume and the built-in ratio and both impacts are investigated in this section.

Variation of the built-in ratio

In **Figure 5.12**, the isentropic efficiency is plotted with respect to the pressure ratio for two vapor qualities. The built-in ratio of the curve with the vapor quality equal to 0.5 is varied to study its impact. In this Figure, the optimal pressure ratio (r_p^*) is equal to 3.2 for a single-phase flow which is not the case for the two-phase flow. One can see that by decreasing the built-in ratio for the two-phase flow, its optimal pressure ratio is getting closer to the one of the single-phase. Indeed, by decreasing $r_{v,in}$, the discharge pressure (P_{in}) increases which leads to less under-expansion.
However, the adaptation of the built-in ratio is different for every vapor quality. Changing the inlet conditions (the expander speed, the inlet pressure,...) also contributes to changing the optimal pressure ratio. To design a two-phase expander, the inlet conditions should be known beforehand.

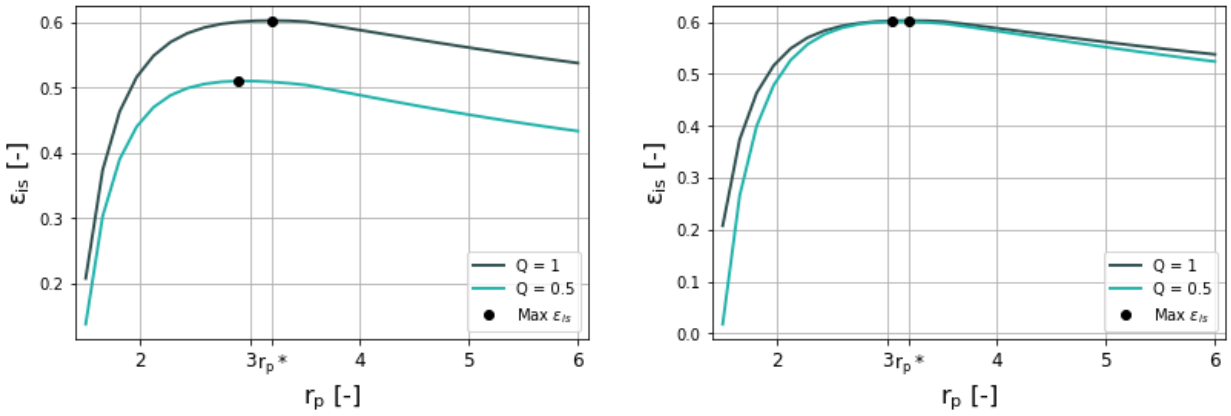

(a) $r_{v,in}$ = *3 for Q = 0.5* **(b)** $r_{v,in}$ = *1.4 for Q = 0.5*

Figure 5.12: *Isentropic efficiency versus the pressure ratio for two vapor qualities and a variation of the built-in ratio ($P_{su} = 6$ bar, N_{exp} = 2600 RPM).*

Variation of the swept volume

In **Figure 5.13**, the isentropic efficiency is represented with respect to the pressure ratio. In **Figure 5.13b**, the swept volume is increased from 86 cm^3 to 150 cm^3 for the two-phase flow. This increase allows the same optimal pressure ratio for both the two-phase and the one-phase flow. The under-expansion losses seem to be attenuated for the two-phase flow.

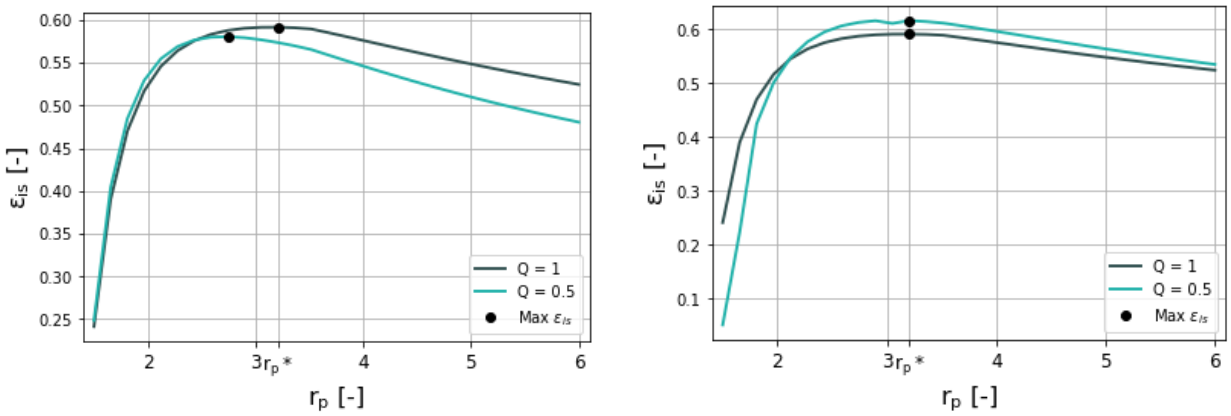

(a) $V_s = 86\ cm^3$ *for both qualities.*

(b) $V_s = 150\ cm^3$ *for Q = 0.5.*

Figure 5.13: *Isentropic efficiency versus the pressure ratio for two vapor qualities and a variation of the swept volume ($P_{su} = 6$ bar, N_{exp} = 2600 RPM)*

5.2 Including the oil properties in the model

As explained in section Section 4.2.2, the oil properties influence greatly the properties of the refrigerant. This section proposed a model to take this effect into account. Unfortunately, due to lack of time, the model has never been able to be fully tested as many errors due to convergence and inexplicable phenomena appeared.

The parameters and the outputs of the model are the same as in the model proposed previously (i.e. Section 5.1.3). The only difference is the addition of the OCR in the inputs of the model.

The mixture properties are determined in a different way than in Section 4.2.2. Indeed, in reality, a portion of the refrigerant is ”trapped” in the oil in its saturated state. This phenomenon can be explained via Raoult's law. Indeed, Raoult's law states that when there is a mixture, the saturation pressure of the mixture is a linear combination of the saturation pressure of the two components (**Equation 5.19**). The oil saturation pressure is very low compared to the one of the refrigerant, which means that the bubble pressure of the mixture is always lower than the saturation pressure of the pure refrigerant.

$$P_{tot} = x_r \cdot P_r^{\sigma}(T) + x_{oil} \cdot P_{oil}^{\sigma}(T) \tag{5.19}$$

Where x_i is the mole fraction of the component i and σ refers to the saturated properties.

The presence of even a small amount of oil in the refrigerant leads to a strong non-azeotropic

behavior. Since the refrigerant/oil mixture is a zeotropic mixture, the saturation temperature and pressure are a function of the oil fraction. The saturation pressure of the mixture decreases with the oil fraction increase. The saturation pressure of oil is very low and one can thus make the assumption that the vapor phase of the mixture is only refrigerant. The thermodynamic model proposed is based on [35]. To model the properties of such a mixture, the following assumptions are made:

- The oil is perfectly miscible in the mixture
- The oil always remains in the liquid form which is a plausible assumption.
- The reference temperature must be identical for both oil and pure refrigerant.

Based on those assumptions, the properties of the mixture (enthalpy, entropy or specific volume) can be evaluated as:

$$X_{mix} = Q \cdot X_{r,vap}(T,P) + OCR \cdot X_{oil}(T) + (1 - Q - OCR) X^{\sigma}_{r,liq}(T) \tag{5.20}$$

Where X represents any properties, *Vap* and *Liq* respectively refer to the vapor and the liquid phases. $OCR = \frac{m_{oil}}{m_{tot}} = \frac{m_{oil}}{m_r + m_{oil}}$ and $Q = \frac{m_{r,vap}}{m_{tot}}$.

The *CoolProp* library can only be used to assess the refrigerant properties. The mixture properties must be determined at each step of the semi-empirical model. However, to determine them, the temperature, the pressure and the vapor quality must be known. Those properties are not known at each step as sometimes, the enthalpy, the entropy or the specific volume of the mixture is conserved. In those cases, an equation is missing, and Raoult's law is used.

For example, to evaluate the isentropic enthalpy of the mixture, the entropy of the mixture ($s_{su,mix}$) is known as well as the exhaust pressure (P_{ex}). The isentropic temperature (T_{is}) and the isentropic vapor quality (Q_{is}) need to be determined. The system with two equations and two unknowns is available in **Equation 5.21**. The second equation is Raoult's law transformed and neglecting the effect of the saturation pressure of the oil.

$$\begin{aligned} s_{mix,su} &= Q_{is} \cdot s_{r,vap}(T_{is}, P_{ex}) + OCR \cdot X_{oil}(T_{is}) + (1 - Q_{is} - OCR) \cdot s^{\sigma}_{r,liq}(T_{is}) \\ P_{ex} &= \frac{P^{\sigma}(T_{is}) \cdot (1 - O\bar{C}R - \bar{Q}_{is})}{1 - \bar{Q}_{is}} \end{aligned} \tag{5.21}$$

One must be careful that the last equation is using molar quantities instead of mass quantities. The molar mass of the POE32 EMKARATE RL32 MAF has been assumed equal to 500 g/mol, which is an average value for a POE (no data available from the supplier). Then T_{is}, Q_{is} and P_{ex} are known and $h_{ex,is}$ can be determined.

Chapter 6

Conclusion and perspectives

To mitigate climate change issues, the European Union has set out ambitious targets for 2030 and 2050. To reach these goals, the EU developed ”Horizon Europe” which is a funding program to finance research and innovation. In September 2020, Horizon Europe launched one new project ”REGEN-BY-2” which is an energy plant capable of converting any type of thermal Renewable Energy Source into energy vectors such as electric heating and or cooling powers. In this energy plant, two-phase fluid machines are required. This thesis aims at characterizing and predicting the performance of a two-phase scroll expander, necessary for the REGEN-BY-2 cycle.

First, a state-of-the-art on two-phase expander is provided, to give an idea of the behaviour of expanders in the two-phase region. Then, the behaviour of the two-phase scroll expander is studied under different conditions and their impact on the expander performance is assessed. A Gaussian prediction method is used to predict new experimental results within the test range. Finally, a semi-empirical model of a two-phase expander is developed to predict the expander's performances outside of the test range. A semi-empirical model of the expander taking the oil into account is also proposed.

The test bench built to test the two-phase is an ORC. The main operational parameters that affect the expander performance are the vapour quality at the expander inlet, the expander rotational speed, the pressure ratio and the expander inlet pressure. Six different actuators are available to vary those parameters; the hot water and the water flow rate at the evaporator inlet, the ORC pump rotational speed, the expander rotational speed, the cold water temperature and the water flow rate at the condenser inlet. The main conclusions withdrawn from the experimental results are that the isentropic efficiency decreases with decreasing vapour quality, which was to be expected. Indeed, when working with a two-phase flow several losses happen such as an increase in the pressure losses in the suction/discharge ports due to the increase in density, there's also a loss of work due to this increase in density. The volumetric efficiency also decreases with decreasing vapor quality, although it seems less im-

pacted because even though two-phase expansion increases pressure losses, leakages should be minimised as the liquid is supposed to act as a ”sealant”. Another observation is that the under-expansion losses appear to be emphasised when working with lower vapour quality. The built-in volume ratio is indeed not adapted to work with two-phase flow.

The experimental results are then used to calibrate the semi-empirical model of the two-phase expander. The calibration doesn't match perfectly the experimental results due to a problem in the vapour quality measurements, and this must be taken into account when interpreting the results. The model is then used to investigate how changing the geometry of the expander could improve its performance for its two-phase application. The main conclusion is that decreasing the expander built-in ratio seem to decrease the under-expansion losses of the two-phase flow.

To conclude this work, perspectives on improvements are provided. The first one is the verification of the calibration of the Coriolis for the density measurements. Indeed, an issue was detected when calibrating the semi-empirical model for the mass flow rate and the problem seemed to come from the heat balance over the evaporator, used to calibrate the Coriolis. Another perspective would be to perform more experimental tests to have a bigger test range. Indeed, the Gaussian prediction has some overfitting due to a lack of experimental data. Other oil circulation ratios could also be tested to evaluate their impact on the expander's performance. Another possible improvement is to include the oil properties in the semi-empirical model. Due to lack of time, this model has never been completed, however, this could help predict better the experimental data.

Bibliography

[1] *Renewable energy targets*. [Online]. Available: https://energy.ec.europa.eu/topics/renewable-energy/renewable-energy-directive-targets-and-rules/renewable-energy-targets_en.

[2] *Horizon Europe*, May 2023. [Online]. Available: https://research-and-innovation.ec.europa.eu/funding/funding-opportunities/funding-programmes-and-open-calls/horizon-europe_en.

[3] *REGEN-BY-2 - ext renewable multi-generation technology enabled by two-phase fluids machines*. [Online]. Available: https://www.regen-by-2.eu/.

[4] M. Francesconi, S. Briola, and M. Antonelli, "A review on Two-Phase Volumetric Expanders and their applications," *Applied sciences*, vol. 12, no. 20, p. 10 328, Oct. 2022. DOI: 10.3390/app122010328. [Online]. Available: https://doi.org/10.3390/app122010328.

[5] O. Dumont, A. Parthoens, R. Dickes, and V. Lemort, "Experimental investigation and optimal performance assessment of four volumetric expanders (scroll, screw, piston and roots) tested in a small-scale organic Rankine cycle system," *Energy*, vol. 165, pp. 1119–1127, Dec. 2018. DOI: 10.1016/j.energy.2018.06.182. [Online]. Available: https://doi.org/10.1016/j.energy.2018.06.182.

[6] E. Georges, S. Declaye, O. Dumont, S. Quoilin, and V. Lemort, "Design of a small-scale organic Rankine cycle engine used in a solar power plant," *International Journal of Low-carbon Technologies*, vol. 8, no. suppl 1, pp. i34–i41, May 2013. DOI: 10.1093/ijlct/ctt030. [Online]. Available: https://doi.org/10.1093/ijlct/ctt030.

[7] S. Briola, P. Di Marco, and R. Gabbrielli, "Two-Phase Fluid Expanders—A Review.," *In Proceedings of the XXX Heat Transfer Conference of Union Italian Thermo-Fluid Dynamic (UIT),*, Jun. 2012.

[8] H. Kanno and N. Shikazono, "Experimental and modeling study on adiabatic two-phase expansion in a cylinder," *International Journal of Heat and Mass Transfer*, vol. 86, pp. 755–763, Jul. 2015. DOI: 10.1016/j.ijheatmasstransfer.2015.02.059. [Online]. Available: https://doi.org/10.1016/j.ijheatmasstransfer.2015.02.059.

[9] S. Lecompte, M. Van Den Broek, and M. De Paepe, "Initial design of an Optical-Access piston expansion chamber for Wet-Expansion," *Energy Procedia*, vol. 129, pp. 307–314, Sep. 2017. DOI: 10.1016/j.egypro.2017.09.195. [Online]. Available: https://doi.org/10.1016/j.egypro.2017.09.195.

[10] O. Dumont, S. Quoilin, and V. Lemort, "Design, Modeling and Experimentation of a Reversible HP-ORC Prototype," *Paper presented at ASME TURBO EXPO 2014*, Jun. 2014. DOI: 10.1115/gt2014-26854. [Online]. Available: https://doi.org/10.1115/gt2014-26854.

[11] V. Lemort, S. Declaye, and S. Quoilin, "Experimental characterization of a hermetic scroll expander for use in a micro-scale Rankine cycle," *Proceedings of the Institution of Mechanical Engineers, Part A: Journal of Power and Energy*, vol. 226, no. 1, pp. 126–136, Feb. 2012. DOI: 10.1177/0957650911413840. [Online]. Available: https://doi.org/10.1177/0957650911413840.

[12] H. J. Huff, D. W. Lindsay, and R. Radermacher, "Positive Displacement Compressor And Expander Simulation," *In Proceedings of the International Compressor Engineering Conference,*, Jan. 2002. [Online]. Available: https://docs.lib.purdue.edu/cgi/viewcontent.cgi?article=2526&context=icec.

[13] D. Westphalen and J. Dieckmann, "Scroll Expander for Carbon Dioxide Cycle," *In Proceedings of the International Compressor Engineering Conference,*, Jul. 2006. [Online]. Available: https://docs.lib.purdue.edu/cgi/viewcontent.cgi?article=1786&context=iracc.

[14] H. Kohsokabe, S. Funakoshi, and K. Tojo, "Operating characteristics of CO2 chiller cycles with expander-compressor unit.," *Appl. Therm. Eng.*, vol. 28, pp. 1654–1661, Sep. 2008. [Online]. Available: https://iifiir.org/fr/fridoc/25788.

[15] M. Fukuta, T. Yanagisawa, O. Kosuda, and Y. Ogi, "Performance of Scroll Expander for CO2 Refrigeration Cycle," *In Proceedings of the International Compressor Engineering Conference, West Lafayette,*, Jan. 2006. [Online]. Available: https://docs.lib.purdue.edu/cgi/viewcontent.cgi?article=2767&context=icec.

[16] A. Hiwata, A. Ikeda, T. Morimoto, O. Kosuda, and M. Matsui, "Axial and radial force control for a CO2 scroll expander," *Science And Technology For The Built Environment*, vol. 15, no. 4, pp. 759–770, Jul. 2009. DOI: 10.1080/10789669.2009.10390862. [Online]. Available: https://doi.org/10.1080/10789669.2009.10390862.

[17] H. J. Kim, J.-M. Ahn, and S. O. Cho, "Numerical simulation on scroll expander-compressor unit for CO2 transcritical cycles.," *Appl. Therm. Eng.*, pp. 28, 1654–1661. 2008. [Online]. Available: https://iifiir.org/fr/fridoc/23942.

[18] M. Kakuda, H. Nagata, and F. Ishizono, "Development of a scroll expander for the CO2 refrigeration cycle," *Science And Technology For The Built Environment*, vol. 15, no. 4, pp. 771–783, Jul. 2009. DOI: 10.1080/10789669.2009.10390863. [Online]. Available: https://doi.org/10.1080/10789669.2009.10390863.

[19] H. J. Kim, J. M. Ahn, I. Park, and P. C. Rha, "Scroll expander for power generation from a low-grade steam source," *Proceedings of the Institution of Mechanical Engineers, Part A: Journal of Power and Energy*, vol. 221, no. 5, pp. 705–711, Jan. 2007. DOI: 10.1243/09576509jpe392. [Online]. Available: https://doi.org/10.1243/09576509jpe392.

[20] R. Zogg and K. Mayer, "Research, development and demonstration of Micro-CHP Systems for Residential Applications - Phase I," Tech. Rep., Mar. 2011. DOI: 10.2172/902084. [Online]. Available: https://doi.org/10.2172/902084.

[21] *Steam Screw Expanders — Xinran*. [Online]. Available: http://www.xinrancompressor.com/7-2-steam-screw-expanders.html.

[22] R. S. Sprankle, "Electrical Power Generating Systems.," *U.S. Patent 3,751,673*, Aug. 1973.

[23] I. K. Smith, N. Stosic, and C. A. Aldis, "Development of the Trilateral Flash Cycle System: Part 3: The Design of High-Efficiency Two-Phase Screw Expanders," *Proceedings of the Institution of Mechanical Engineers, Part A: Journal of Power and Energy*, vol. 210, no. 1, pp. 75–93, Feb. 1996. DOI: 10.1243/pime\{_}proc\{_}1996\{_}210\{_}010\{_}02. [Online]. Available: https://doi.org/10.1243/pime_proc_1996_210_010_02.

[24] S. I.K. and S. K, "Screw expanders increase output and decrease the cost of geothermal binary power plant systems.," *In Proceedings of the Geothermal Research Council Annual Meeting, Reno, NV, USA, 25–28*, Sep. 2005.

[25] S. I.K., S. N., and K. A., "Cost effective small scale ORC systems for power recovery from low enthalpy resources.," *In Proceedings of the Geothermal Research Council Annual Meeting, Reno, NV, USA*, 2007.

[26] M. Read, N. Stosic, and I. K. Smith, "Optimization of screw expanders for power recovery from Low-Grade heat sources," *Energy technology and policy*, vol. 1, no. 1, pp. 131–142, Jan. 2014. DOI: 10.1080/23317000.2014.969454. [Online]. Available: https://doi.org/10.1080/23317000.2014.969454.

[27] H. Vasuthevan and A. Brummer, "Thermodynamic modelling of screw expander in a Trilateral Flash cycle.," *In Proceedings of the International Compressor Engineering Conference, West Lafayette, IN, USA,*, Jul. 2016.

[28] A. Nikolov and A. Brümmer, "Impact of different clearance heights on the operation of a water-flooded twin-screw expander—experimental investigations based on indicator diagrams," *IOP conference series*, vol. 425, p. 012 008, Nov. 2018. DOI: 10.1088/1757-899x/425/1/012008. [Online]. Available: https://doi.org/10.1088/1757-899x/425/1/012008.

[29] G. Bianchi, M. Marchionni, J. Miller, and S. A. Tassou, "Modelling and off-design performance optimisation of a trilateral flash cycle system using two-phase twin-screw expanders with variable built-in volume ratio," *Applied Thermal Engineering*, vol. 179, p. 115 671, Oct. 2020. DOI: 10.1016/j.applthermaleng.2020.115671. [Online]. Available: https://doi.org/10.1016/j.applthermaleng.2020.115671.

[30] I. Tamura, H. Taniguchi, H. Sasaki, R. Yoshida, I. Sekiguchi, and M. Yokogawa, "An analytical investigation of high-temperature heat pump system with screw compressor and screw expander for power recovery," *Energy Conversion and Management*, vol. 38, no. 10-13, pp. 1007–1013, Jul. 1997. DOI: 10.1016/s0196-8904(96)00130-6. [Online]. Available: https://doi.org/10.1016/s0196-8904(96)00130-6.

[31] J. J. Brasz, I. K. Smith, and N. Stosic, "Development of a Twin Screw Expressor as a Throttle Valve Replacement for Water-Cooled Chillers," *In Proceedings of the International Compressor Engineering Conference, West Lafayette, IN, USA,*, Jan. 2000. [Online]. Available: http://www.staff.city.ac.uk/~ra601/brasz.pdf.

[32] A. Kovacevic, N. Stosic, I. F. C. Smith, and I. F. C. Smith, *Power Recovery from Low Grade Heat by Means of Screw Expanders*. Jan. 2014. DOI: 10.1016/c2013-0-23224-4. [Online]. Available: https://doi.org/10.1016/c2013-0-23224-4.

[33] S. Sholahudin, K. Ohno, S. Yamaguchi, and K. Saito, "Multi-step ahead prediction of vapor compression air conditioning system behaviour using neural networks," *IOP conference series*, Jun. 2019. DOI: 10.1088/1757-899x/539/1/012003. [Online]. Available: https://doi.org/10.1088/1757-899x/539/1/012003.

[34] D. L. Rudnick, "Ocean Research Enabled by Underwater Gliders," *Annual Review of Marine Science*, vol. 8, no. 1, pp. 519–541, Jan. 2016. DOI: 10.1146/annurev-marine-122414-033913. [Online]. Available: https://doi.org/10.1146/annurev-marine-122414-033913.

[35] M. Youbi-Idrissi and J. Bonjour, "The effect of oil in refrigeration: Current research issues and critical review of thermodynamic aspects," *International Journal of Refrigeration-revue Internationale Du Froid*, vol. 31, no. 2, pp. 165–179, Mar. 2008. DOI: 10.1016/j.ijrefrig.2007.09.006. [Online]. Available: https://doi.org/10.1016/j.ijrefrig.2007.09.006.

[36] M. Youbi-Idrissi, J. Bonjour, C. Marvillet, and F. Meunier, "Impact of refrigerant–oil solubility on an evaporator performances working with R-407C," *International Journal of Refrigeration-revue Internationale Du Froid*, vol. 26, no. 3, pp. 284–292, May 2003. DOI: 10.1016/s0140-7007(02)00129-9. [Online]. Available: https://doi.org/10.1016/s0140-7007(02)00129-9.

[37] H. Matsumoto, C. Jones, H. Klinck, D. K. Mellinger, R. P. Dziak, and C. Meinig, "Charge-sensitive methods for the off-design performance characterization of organic rankine cycle (orc) power systems.," *The Journal of the Acoustical Society of America*, vol. 133, no. 2, p. 731, 2013, ISSN: 00014966. DOI: 10.1121/1.4773260.

[38] S. Quoilin and J. Schrouff, "Assessing Steady-State, multivariate experimental data using Gaussian processes: the GPEXP Open-Source Library," *Energies*, vol. 9, no. 6, p. 423, May 2016. DOI: 10.3390/en9060423. [Online]. Available: https://doi.org/10.3390/en9060423.

[39] *3.1. Cross-validation: evaluating estimator performance*. [Online]. Available: https://scikit-learn.org/stable/modules/cross_validation.html.

[40] S. Quoilin, *GitHub - squoilin/GPExp: A Gaussian Processes framework for the analysis of Experimental Data*. [Online]. Available: https://github.com/squoilin/GPExp.

[41] V. Lemort, "Contribution to the Characterization of Scroll Machines in Compressor and Expander Modes," *Nope*, Dec. 2008. [Online]. Available: http://orbi.ulg.ac.be/handle/2268/135317.

[42] Y. Chen, N. P. Halm, E. A. Groll, and J. E. Braun, "Mathematical modeling of scroll compressors—part I: compression process modeling," *International Journal of Refrigeration-revue Internationale Du Froid*, vol. 25, no. 6, pp. 731–750, Sep. 2002. DOI: 10.1016/s0140-7007(01)00071-8. [Online]. Available: https://doi.org/10.1016/s0140-7007(01)00071-8.

[43] V. Lemort, G. Olivier, and G. De Pelsemaeker, *Thermal energy management in vehicles*. John Wiley and Sons, Mar. 2023.